Performance optimization of lead-free $(CH_3NH_3)_3Bi_2I_9$-based perovskite solar cell: A SCAPS-1D simulation study

A DISSERTATION

SUBMITTED IN PARTIAL FULFILLMENT OF THE REQUIREMENTS

FOR THE AWARD OF THE DEGREE

OF

MASTER OF SCIENCE

IN

PHYSICS

Submitted by:

SUDHIR KUMAR

(23/MSCPHY/46)

Under the supervision of

Dr. SARITA BAGHEL
Assistant Professor

DEPARTMENT OF APPLIED PHYSICS

DELHI TECHNOLOGICAL UNIVERSITY

(Formerly Delhi College of Engineering)

Bawana Road, Delhi- 110044, India

MAY, 2025

DECLARATION

I hereby certify that the work which is presented in Project Dissertation-II entitled **"Performance optimization of lead-free $(CH_3NH_3)_3Bi_2I_9$-based perovskite solar cell: A SCAPS-1D simulation study"** in fulfillment of the requirements for the award of the Degree of **Master of Science in Physics** and submitted to the Department of Applied Physics, Delhi Technological University, Delhi, is an authentic record of my own, carried out during a period from August 2024 to May 2025, under the supervision of **Dr. Sarita Baghel**.

The matter presented in this thesis has not been submitted by me for the award of any other degree of this or any other Institute/University. The work has been submitted in SCI/SCI expanded/SSCI/Scopus indexed journal with the following details:

Title of the paper: Performance optimization of lead-free $(CH_3NH_3)_3Bi_2I_9$-based perovskite solar cell: A SCAPS-1D simulation study

Author names (in sequence as per research paper): Sudhir Kumar[*], Rahul Kundara, and Sarita Baghel[1]

Name of Journal: Transactions on Electrical and Electronic Materials (TEEM), Springer.
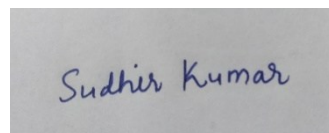**Status of paper (Accepted/Published/Communicated):** Communicated
Date of paper communication: May 5, 2025
Date of paper acceptance: N/A
Date of paper publication: N/A

Place: Delhi
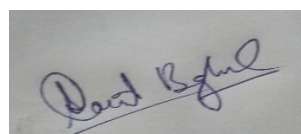**Date:** 09 June 2025   **Sudhir Kumar (23/MSCPHY/46)**

SUPERVISOR CERTIFICATE

To the best of my knowledge, the above work has not been submitted in part or full for any Degree or Diploma to this University or elsewhere. I, further certify that the publication and indexing information given by the student is correct.

Place: Delhi   **Dr. Sarita Baghel**
Date: 09 June 2025   **SUPERVISOR**
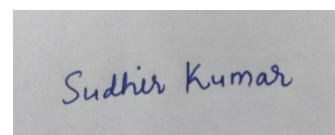
ABSTRACT

Perovskite solar cells (PSCs) have captured widespread recognition in the photovoltaic field because of their superior efficiency and affordable manufacturing. The toxicity of lead-based perovskites poses environmental concerns. In this context, the Pb-free perovskite methylammonium bismuth iodide $(CH_3NH_3)_3Bi_2I_9$ presents a viable alternative to the Pb-based halide cells, offering a harmless nature and exceptional durability. We have investigated the intrinsic impacts of $(CH_3NH_3)_3Bi_2I_9$ perovskite by employing SCAPS-1D. We optimised different variables, including thickness, Defect Density N_t, energy bandgap, Temperature, and carrier density for ETL and HTL, which affect a PSC's performance. We also investigated the effect of diverse HTLs and ETLs on the device's performance. The simulation results show an efficiency of 18.14 % with V_{oc} of 1.67 V, J_{sc} of 12.72 mA/cm^2 and FF of 85.16 %, for the configuration FTO/WS$_2$/MA$_3$Bi$_2$I$_9$/NiO/Pt, with a Thickness of 500 nm and Defect D. (N_t) of 10^{14} cm^{-3}, at a Temperature of 300K. These findings suggest that $(CH_3NH_3)_3Bi_2I_9$ material is a promising prospect for future sustainable solar energy technology.

ACKNOWLEDGEMENT

I am sincerely grateful to my dissertation Supervisor, **Dr. Sarita Baghel,** for their invaluable support, thoughtful advice, and constant encouragement while working on my research project. Their mentorship has guided my work in the right direction and helped me grow both academically and personally. I am also sincerely thankful to the faculty of the Department of Applied Physics at Delhi Technological University for creating an encouraging academic atmosphere and also offering vital resources. I would especially like to thank my Ph.D. scholar, **Dr. Rahul Kundara**, for their generous support, insightful suggestions, and steady motivation, which have made a significant difference in this project. Finally, I would like to express my heartfelt appreciation to my parents. Their selfless love and continual support have guided and empowered me throughout my academic journey.

Place: Delhi

Date: 09 June 2025

SUDHIR KUMAR

CONTENTS

LIST OF FIGURES

Figure: 3.1 Diagrammatic representation of the fundamental steps involved in the SCAPS-1D simulator.

Figure: 3.2 Standard device structure of PSC with different layers.

Figure: 4.1 Band diagram of different ETL materials with $(CH_3NH_3)_3Bi_2I_9$ as an absorber layer

Figure: 4.2 Band diagram of $(CH_3NH_3)_3Bi_2I_9,$ as an absorber layer with different HTL Materials

LIST OF TABLES

LIST OF SYMBOLS AND ABBREVIATIONS

S. No.	Symbols	Meaning or full form
1	η	Power conversion efficiency
2	J_{SC}	Short-circuit current density
3	V_{OC}	Open-circuit voltage
4	FF	Fill factor
5	ε_r	Dielectric constant
6	χ	Electron affinity
7	μ_e	Electron Mobility
8	μ_h	Hole Mobility
9	N_D	Donor Density
10	N_A	Acceptor Density
11	Nt	Total density
12	Eg	Energy band gap

S. No.	Abbreviated words	Full-length or (full form)
1	ETL	Electron transport layer
2	HTL	Hole transport layer
3	FTO	Fluorine-Doped Tin Oxide (Electrode)
4	MBI	Methyl Bismuth Iodide
5	WS_2	Tungsten disulfide
6	NiO	Nickel Oxide
7	Pt	Platinum (Electrode)
8	PCBM	Phenyl-C_{61}-butyric acid Methyl ester
9	PEDOT: PSS	Poly(3,4-ethylenedioxythiophene): Poly (Styrene sulfonate)
10	ZnSe	Zinc Selenide
11	IGZO	Indium Gallium Zinc Oxide
12	TiO_2	Titanium dioxide
13	PSC	Perovskite Solar Cell
14	DPSC	Double perovskite solar cell
15	SCAPS-1D	Solar Cell Capacitance Simulator – 1 Dimension

CHAPTER:1

Introduction

Imagine a world where every rooftop, window, or even backpack could generate clean, renewable electricity from sunlight. This is no longer a distant dream thanks to the rapid evolution of solar technology. As the global population grows and the effects of climate change become increasingly urgent, the need for sustainable and accessible energy solutions has never been clearer. Among the many contenders in the race toward a greener future, solar cells devices that convert sunlight directly into electricity have taken centre stage.

Traditional solar technologies, especially those based on crystalline silicon, have been instrumental in bringing solar power to homes, industries, and even satellites. These cells work through a beautifully simple process: when sunlight hits a semiconductor material, it energizes electrons enough to set them free, generating an electric current that can power anything from a calculator to a city. Over the years, these cells have become more efficient and more affordable, but they are still limited by material costs, energy-intensive manufacturing, and physical rigidity. Then, something revolutionary happened. In 2009, researchers experimenting with a new class of materials discovered that a crystal structure known as perovskite could also convert sunlight into electricity, and remarkably well. What started as a niche laboratory curiosity has rapidly blossomed into one of the most exciting frontiers in solar energy. Today, Perovskite Solar Cells **(PSCs)** are turning heads across the scientific community for their exceptional light-harvesting abilities, low-cost production potential, and surprising flexibility.

Perovskite materials are special not only because they work but because they work so well. In just over a decade, their efficiency has skyrocketed from under 4% to over 25%, putting them in direct competition with silicon. And they do this with a fraction of the material, on flexible surfaces, and with far less energy required to manufacture. Imagine printing solar panels like newspapers or integrating them into lightweight fabrics perovskites make these futuristic ideas surprisingly feasible.

What makes them so powerful? Structurally, perovskites have a unique arrangement (commonly written as ABX_3) that allows for excellent light absorption, long electron lifetimes, and easy tuning of their properties. The most studied perovskites, typically based on lead halides, absorb a broad spectrum of sunlight and generate electricity efficiently even

under low light conditions. Better yet, they can be layered on top of traditional silicon cells in tandem configurations, pushing the boundaries of solar efficiency even further.

This thesis dives into the fascinating world of perovskite solar cells—from their fundamental chemistry and working principles to the cutting-edge advances that are shaping their future. It will explore the challenges, innovations, and opportunities that define this dynamic field, with the hope that PSCs might one day transform how the world captures and uses solar energy. We are standing at the edge of a solar revolution. And perovskites might just be the material that takes us over the threshold.

PSCs have acquired recognition in the P-V industry owing to their excellent efficiency, cost-effective fabrication, and easy synthesis process [1]. The research field of solar cells has been greatly influenced by organic-inorganic PSCs due to their outstanding attributes, such as high charge carrier mobility, high absorptivity, an increased dielectric constant, desired deposition through solution processing method, cost-effective manufacturing, and low-heat deposition unlike traditional silicon-based photovoltaic devices [2]. The huge improvement in efficiency and stability in PSCs can be seen in just 10 years. The perovskite material was used for the first time in solar cells as documented by Miyasaka and colleagues in 2009, achieving a PSC of 3.8 % [3]. The Pb-based perovskite solar cells cause serious issues with their sustainability due to their toxic nature, which is highly harmful to both the environment and living organisms. Furthermore, Pb-based perovskites suffer from a stability problem because of the rapid oxidation of the Pb^{2+} cation under atmospheric conditions such as moisture, dust, and other factors. To eliminate the toxicity and stability issues faced by PSC, researchers have explored numerous ways to exchange the Pb with elements such as Sb, Sn, Bi, double perovskite, etc. Replacing the Pb^{2+} cation with Sn^{2+}, which has a similar divalent crystal structure, does not alter the composition of PSCs as Sn^{2+} has a smaller radius than Pb^{2+} cation. The Sn-based perovskites also have narrow band gaps, making them theoretically more efficient than the Pb-based perovskite solar cells. $CsSnI_3$ was employed in 2012, as reported by Chen et al. [4]; however, the efficiency was reportedly just 0.9%. Subsequently, caesium (Cs) was replaced with the (CH_3NH_3) by Noel et al. with PCE 6% [5]. However, tin (Sn)-based solar cells are still facing the problem of stability due to their ambient environmental factors as rapid oxidation from Sn^{2+} to Sn^{4+} [5,6]. To address toxicity and enhance stability, hetero-valent materials like Bi and Sb have been experimentally tested in laboratories to evaluate their suitability and durability for use in perovskite solar cells. These hetero-valent materials, such as Bi^{3+} and Sb^{3+}, exhibit a stable oxidation state

comparable to homo-valent materials like Pb, Sn, and Ge. However, Bi^{3+} exhibits superior electro-optical properties compared to Pb^{2+}, owing to their similar properties, such as ion size and electronic configuration of these materials. Recent studies indicate that Bi-based perovskites such as $(CH_3NH_3)_3Bi_2I_9$, also known as methylammonium bismuth iodide (MBI), are promising candidates for use as light-harvesting layers in PSCs [7]. Previously, the Bi-based perovskite solar cell PSC had investigated both theoretical and experimental ways [8-10]. The $(CH_3NH_3)_3Bi_2I_9$, is perovskite material in which the organic part of perovskite $(CH_3NH_3)^{3+}$ cation is introduced to maintain charge neutrality in the PSC structure, Bi^{3+} ion acts as the central metal atom that replaces Pb^{2+} ion while iodide ion forms octahedral co-ordination around the Bi^{+3} ion and generating a linkage that supports the perovskite material [11]. Researchers have demonstrated keen attention to bismuth-based perovskite materials owing to exceptional electronic properties, non-toxic nature, and outstanding durability in moist environments. Take a look at some previous studies on bismuth-based perovskite materials. Senol Öz and Jan-Christoph H. reported a wide bandgap $(CH_3NH_3)_3Bi_2I_9$ perovskite utilized as a light-responsive layer in PSCs. They observed a conversion rate of around 0.1% for the flat p-i-n PSC [12]. Fengzhu Li and Haochen Fan employ the lead-free uniform and tightly packed MBI films using the two PSCs. The lead-free MBI films were manufactured by using a two-step deposition method. This MBI film obtained a better efficiency of 0.33% [13]. The novelty of $(CH_3NH_3Bi_2I_9)$ lies in its potential as a harmless, environment-friendly alternative for Pb-based perovskite materials in solar cells. In this study, numerical modelling is conducted using SCAPS-1D software to optimise ETL and HTL with the $CH_3NH_3Bi_2I_9$ perovskite layer, aiming to determine the best configuration for achieving a high-performance device. We also optimized several parameters like defect density, thickness, operating temperature, energy bandgap of the perovskite layer, and carrier density of ETL and HTL to improve device performance. During the simulation, it was observed that the PSC model, designated as $FTO/WS_2/CH_3NH_3Bi_2I_9/NiO/Pt$, achieved a maximum efficiency of 18.14 % with Voc of 1.67 V, Jsc of 12.72 mAcm^{-2}, and a Fill factor of 85.16 %. This efficiency is approximately double the previous results of 9.04%, as shown in Table 4.4, Furthermore, the incorporation of a suitable Metal contact with a work function of 5.65 eV [14] contributed to this enhanced performance.

CHAPTER: 2

Literature Review

2.1 Background Knowledge

As the world races to embrace cleaner energy sources, solar power has taken centre stage in the push for sustainability. Among the most exciting breakthroughs in this area are perovskite solar cells (PSCs), a class of materials that has completely reshaped what we thought was possible in solar energy. What makes them so special is their unique **ABX$_3$** crystal structure, which allows them to absorb sunlight remarkably well and convert it into electricity with high efficiency. Since their introduction in 2009, PSCs have improved from a humble **3.8%** efficiency to over **26%** in the lab, one of the fastest rises in performance seen in any solar technology.

This leap in efficiency has been driven by clever innovations in how the cells are designed, from smarter device architectures and better charge transport layers to simpler and more scalable manufacturing techniques. However, there's a downside: most high-efficiency PSCs contain lead (Pb), which poses health and environmental risks. Moreover, these materials tend to degrade when exposed to heat, moisture, or sunlight, a major problem for solar panels meant to last for decades outdoors.

To solve these problems, researchers have been developing lead-free alternatives, with a lot of attention now turning to a newer class called double perovskite solar cells (DPSCs). These materials replace toxic lead with safer elements like bismuth (Bi), silver (Ag), and tin (Sn), etc, and offer better stability under real-world conditions. One promising example is **Cs$_2$BiAgI$_6$**, which has shown good potential in early studies. In theory, DPSCs could reach efficiencies of **27%** or more, but in practice, they're still playing catch-up with lead-based cells, often stuck around 15–20%. That gap is due to a mix of issues, including less efficient charge movement, defects at layer interfaces, and energy lost through the recombination of charge carriers.

This is where a new generation of double perovskite materials comes in. Compounds like **Cs$_3$Bi$_2$I$_9$, MA$_3$Bi$_2$I$_9$, FA$_3$Bi$_2$I$_9$, MASnI$_3$, FASnI$_3$, Cs$_2$AgBiBr$_6$**, and **Cs$_2$AgBiCl$_6$** have been successfully synthesized and show real promise. They are **non-toxic**, **chemically stable**, and have suitable band gaps for harvesting solar energy. Among these, Cs$_3$Bi$_2$I$_9$ stands out as especially promising. It's not only safe for the environment, but also fairly stable when

exposed to light and air. Researchers have found that adding small amounts of potassium iodide (KI) during the manufacturing process improves the crystal quality and helps reduce flaws that would otherwise hurt efficiency. Thanks to such tweaks, some devices have now reached **2.81%** efficiency, which, while modest, is a step in the right direction.

$MA_3Bi_2I_9$ is another strong candidate. It's also stable and eco-friendly, and current studies are focused on improving its composition and fabrication methods to boost both performance and durability. Researchers are experimenting with new solvents, additives, and layer designs to fine-tune how these materials behave inside a solar cell.

To make DPSCs truly practical, the focus is also shifting toward building devices that are not only efficient but also durable and scalable. For example, inorganic materials like SnO_2 and NiO are being explored for use as charge transport layers, offering better stability than their organic counterparts. New Protective strategies**,** ways of sealing the cells against moisture and UV damage, are also showing promise. On the production side, techniques like slot-die coating allow for larger, uniform films that can be mass-produced without sacrificing too much efficiency.

Excitingly, researchers are also using machine learning to predict which material combinations and layer structures will work best. These tools help speed up discovery and reduce trial-and-error in the lab. And on the frontier of solar tech, tandem solar cells, where DPSCs are layered with other solar materials, are being explored to push overall efficiencies above **30%**. Figuring out how to combine these materials effectively is still a challenge, but the potential payoff is huge.

In short, while perovskite and double perovskite solar cells have already made a big splash in the world of solar research, the journey from the lab to your rooftop is still ongoing. Tackling the tough questions around efficiency, stability, and scalability will be key to turning these exciting materials into the next generation of mainstream, clean energy solutions.

2.2 Purpose of Research

This research is motivated by the vision of creating solar technologies that are not only efficient but also safe for both people and the environment. At the heart of this project is methylammonium bismuth iodide ($MA_3Bi_2I_9$), a lead-free perovskite material that holds great promise as an alternative to conventional, lead-based perovskite solar cells. While traditional perovskites have set new benchmarks in solar cell efficiency, their reliance on toxic lead has raised significant concerns about environmental safety and long-term health risks. Our work aims to bridge this gap by demonstrating that $MA_3Bi_2I_9$ can combine strong photovoltaic performance with a non-toxic, environmentally friendly profile.

The primary goal is to show that solar cells based on $MA_3Bi_2I_9$ can achieve efficiencies and operational stability comparable to their lead-based counterparts. To do this, we are focusing on optimizing the material's composition to improve light absorption, refining fabrication techniques for better film quality, and designing device architectures that minimize energy losses. Recognizing that solar panels must endure real-world conditions, we are also working to enhance the durability of $MA_3Bi_2I_9$ cells by developing moisture-resistant coatings and robust charge transport layers. Another key aspect of this research is to make these advances scalable, so that the technology can move beyond laboratory prototypes to large-area modules suitable for widespread use. This involves exploring cost-effective manufacturing methods, such as inkjet printing and roll-to-roll processing, to ensure that $MA_3Bi_2I_9$ solar cells can be produced efficiently and at scale.

Finally, we are addressing the common limitations of bismuth-based perovskites, such as suboptimal film morphology and limited charge mobility, by experimenting with additives, interface engineering, and structural modifications. Ultimately, this research seeks not just to improve a material but to redefine what sustainable solar energy can be, offering a solution that is both powerful and safe, and helping to pave the way for a cleaner, greener future.

CHAPTER: 3

Materials And Methods

3.1 Novelty of Material

The true novelty of methylammonium bismuth iodide ($MA_3Bi_2I_9$) lies in its potential to fundamentally change how we think about safe and sustainable solar energy. Unlike traditional perovskite materials that rely on lead, raising serious concerns about toxicity and environmental harm, $MA_3Bi_2I_9$ swaps out this hazardous element for bismuth, which is far less risky for both people and the planet. This simple yet powerful substitution means $MA_3Bi_2I_9$ offers a much safer path forward for the widespread adoption of perovskite solar cells. But its advantages don't stop at safety. $MA_3Bi_2I_9$ is also known for its impressive thermal stability and strong crystal structure, both of which are essential for building solar panels that can stand the test of time in real-world conditions. The material's ability to form smooth, high-quality films is another key strength, as it helps maximize the efficiency with which sunlight is converted into usable electricity. Researchers are actively experimenting with different ways to fine-tune the composition and fabrication of $MA_3Bi_2I_9$, aiming to push its performance even closer to that of its lead-based counterparts. By addressing the twin challenges of efficiency and environmental responsibility, MBI stands out as a genuinely innovative material, one that could help make solar energy cleaner, safer, and more accessible for everyone.

3.2 SCAPS-1D Software

- **SCAPS-1D Interface:** The SCAPS startup interface: central action panel
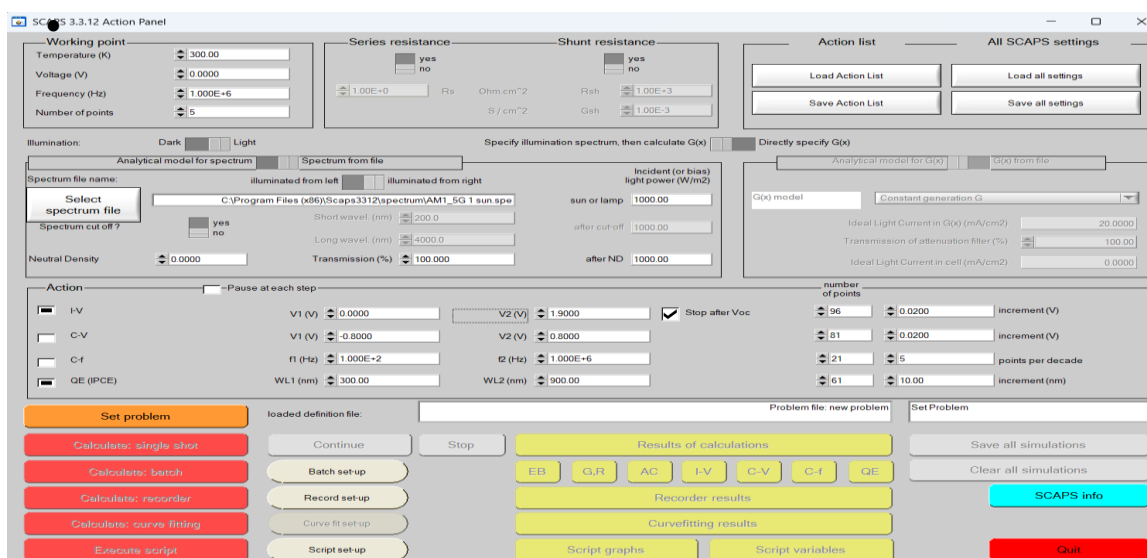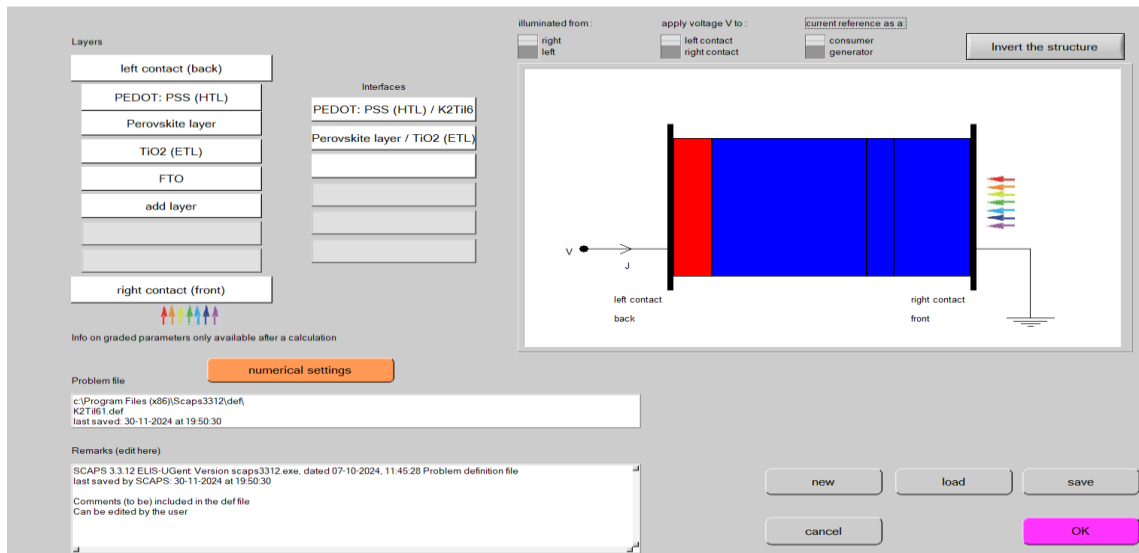
3.2.1: About SCAPS-1D Software

Imagine testing and refining solar cell designs without ever entering a lab. That's the promise of SCAPS-1D, a one-dimensional solar cell simulation program created by the Department of Electronics and Information Systems at the University of Gent, Belgium. Acting as a virtual lab, SCAPS-1D enables researchers to model, analyze, and optimize thin-film solar cells with high precision, streamlining the path from concept to real-world application. It significantly reduces material waste, shortens development time, and lowers research costs, making solar innovation more accessible and sustainable. At its core, SCAPS-1D simulates how light and electricity interact within the layered structure of a solar cell. It focuses on the vertical stack, absorber, buffer, and contact layers, and predicts how material properties, thickness, and defects impact performance. The software solves complex physical equations numerically, providing key outputs like current-voltage (J-V) characteristics, quantum efficiency (QE), and electric field distribution.

SCAPS-1D also models light behaviour using the Transfer Matrix Method (TMM), which tracks how light reflects, transmits, or is absorbed in each layer. This allows for optimizing sunlight capture and minimizing energy losses. Its user-friendly interface and flexible input options make it ideal for both academic research and industrial prototyping. The **two images** above have been sourced from the **SCAPS-1D** software documentation. Beyond its calculations, SCAPS-1D helps engineers virtually test countless design variations, adjusting doping, layer interfaces, and more, to find the best balance between efficiency, durability, and cost. This is especially critical for emerging solar technologies like perovskites, where small tweaks can greatly impact performance.

3.2.2 Basics Action: SCAPS-1D Software

- **Run SCAPS-1D** – Launch the simulator to begin your session.
- **Define the device structure** – Set up the geometry, select materials, and input all necessary physical and electrical properties.
- **Set simulation conditions** – Choose the operating environment or working point, such as illumination, temperature, or voltage.
- **Select the simulation type** – Decide what you want to simulate, like J-V characteristics, C-V curves, or quantum efficiency.
- **Start the simulation** – Execute the selected calculations based on your input setup.
- **View results** – Display and analyze the output curves generated from the simulation.

The schematic diagram illustrates the main steps typically involved in a SCAPS-1D simulation, providing a clear view of the overall process, referenced from [15].
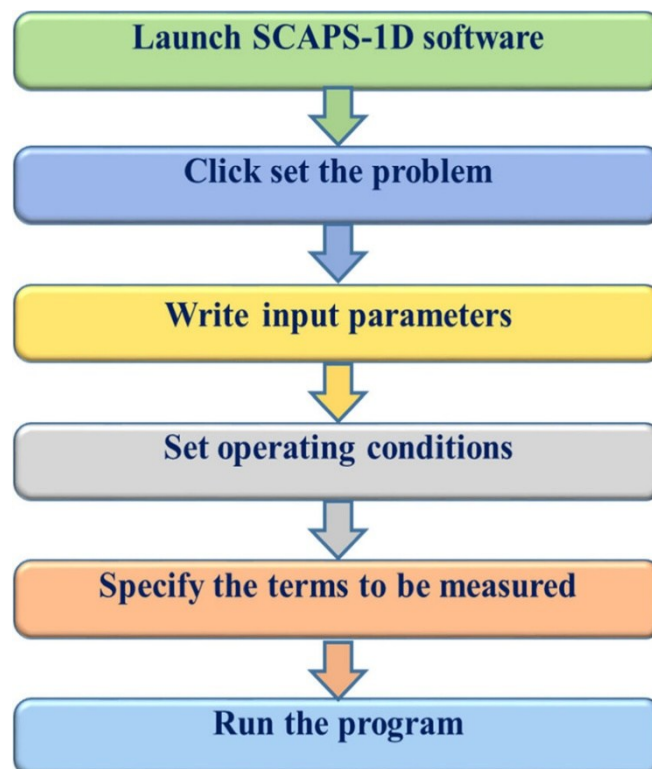
Figure 3.1 Diagrammatic representation of the fundamental steps involved in the SCAPS-1D simulator.

3.3 Numerical Simulation

When designing and understanding solar cells, especially perovskite-based ones, numerical modeling plays a crucial role in predicting how these devices will perform in real-world conditions. For perovskite solar cells, which exhibit intricate and often unpredictable behavior, computational methods serve as an essential bridge between theoretical concepts and practical applications. These simulations help researchers validate their understanding of the underlying physics and predict how modifications to the device structure might affect overall performance.

The SCAPS-1D simulation platform operates by solving fundamental equations that govern charge carrier behavior within the solar cell. These include the equations of continuity for both holes and electrons, along with Poisson's equation, which together describe how charges move, accumulate, and recombine throughout the device. The key equations that SCAPS-1D works with are presented below: [16,17].

$$\frac{dn_n}{dt} = G_p - \frac{p_n - p_{n_0}}{\tau_p} + p_n\mu_p\frac{d\xi}{dx} + \mu_p\xi\frac{dn_n}{ds} + Dp\frac{d^2p_n}{dx^2} \tag{1}$$

$$\frac{dn_p}{dt} = G_n - \frac{n_p - n_{p_0}}{\tau_n} + n_p\mu_n\frac{d\xi}{dx} + \mu_n\xi\frac{dn_n}{ds} + Dn\frac{d^2p_n}{dx^2} \tag{2}$$

$$\frac{d}{dx}\left(\varepsilon(x)\frac{d\phi}{dx}\right) = q[p(x) - n(x) + N_D(x) - N_A(x) + \rho_p - \rho_n] \tag{3}$$

$$J = J_n + J_p$$

$$J_n = D_n\frac{dn}{dx} + \mu_n n\frac{d\phi}{dx} \quad \text{Drift Diffusion Equation for Electrons}$$

$$J_p = Dp\frac{dp}{dx} + \mu_p p\frac{d\phi}{dx} \quad \text{Drift Diffusion Equation for Holes}$$

$$n = N_C \exp\left[\frac{E_C - E_{n_f}}{kT}\right] \quad \text{Concentration of electrons}$$

$$p = Nv \, exp \left[\frac{E_{n_f} - E_v}{kT} \right] \quad \text{Concentration of holes}$$

$$L_{n,p} = \sqrt{D_{n,p} \, \tau_{n,p}} \quad \text{Diffusion length for electrons and holes}$$

$$\tau = \frac{1}{\sigma N_t v_{th}} \quad \text{Charge carrier lifetime}$$

$$R_{SRH} = \frac{pn - n_i^2}{\tau_p(n + n_i) + \tau_n(n + p_i)} \quad \text{Defect-level recombination rate}$$

Where ξ denotes the Electric field, n and p are electron-hole concentrations, ϕ is the electric potential, q represents elementary charge, ε denotes permittivity, N_A and N_D, indicate the charge carrier density of acceptors and donors, while ρ_p and ρ_n represent the hole and electron distributions. R and G are referred to as the recombination rate and generation rate, respectively. J_n and J_p show the electron and hole Current density, D_n and Dp are diffusion coefficients for electrons and holes. Nc & Nv show the DOS of the Conduction and Valence bands. Ec & Ev represent the conduction band and valence band, respectively. The E_{n_f} represents the Fermi energy level, and T indicates the temperature. μ_p and μ_n represent the mobilities of holes and electrons. τ_p and τ_n represents holes and electrons' lifetimes, respectively. Finally, τ is the carrier lifetime, the catch cross-section of the trap is represented by σ, and v_{th} denotes the carrier's thermal velocity.

3.4 Device Structure

The perovskite solar cell configuration investigated in this research follows the structure: FTO/ETL/(CH$_3$NH$_3$)$_3$Bi$_2$I$_9$/HTL/Pt. This design utilizes Fluorine-doped Tin Oxide (FTO) as the transparent front electrode, leveraging its excellent properties as a transparent conductive oxide. The effectiveness of this structure is enhanced through the strategic selection of different ETLs and HTLs.

For the electron transport functionality, this study explores several material options, including TiO$_2$, IGZO, ZnSe, PCBM, and WS$_2$. These materials serve as pathways for electrons to travel efficiently from the active layer to the front contact. Similarly, for hole transport, the investigation includes Cu$_2$O, CuI, NiO, PEDOT: PSS, Spiro-OMeTAD, and

CuSCN as potential HTL materials. The back contact consists of Platinum (Pt), chosen for its favourable Work function of 5.65 eV, which facilitates proficient carrier collection.

Figure 1 demonstrates the standard architecture of the optimized perovskite solar cell, clearly showing the sequential arrangement of FTO, ETL, absorber layer, and HTL components. The illuminated side features FTO configured as a flat-band contact, while the opposite side incorporates the Platinum back contact with its 5.65 eV work function serving as an effective electrode. The material parameters for each layer used in the simulation are carefully selected based on previously published research findings, as detailed in Tables 3.1 and 3.2.

The photo-absorption behaviour of the different layers is calculated using SCAPS-1D's integrated model, which employs equation (4):

$$\alpha = A_a \sqrt{(h\nu - E_g)}$$

Here, 'A_a' represents a material-specific pre-factor that determines the absorption characteristics unique to each layer.
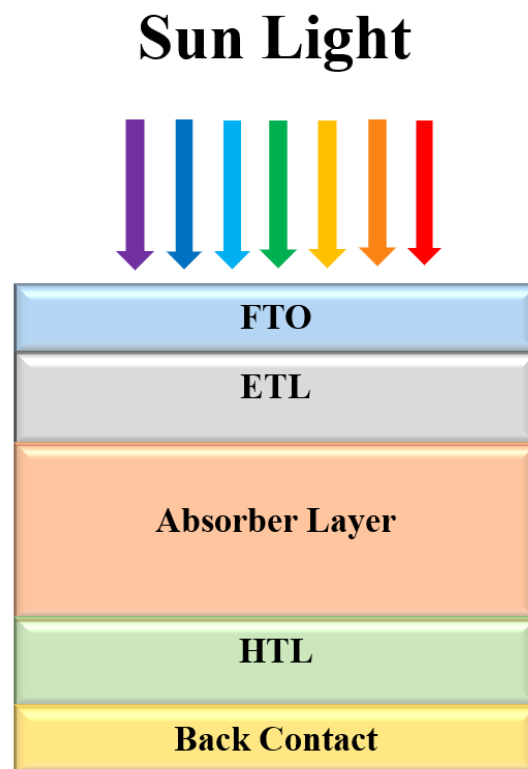

Figure 3.2 Standard device structure of PSC with different layers

Table 3.1: Input parameters of perovskite material, different ETL, and FTO

Parameters	MBI	TiO$_2$	IGZO	PCBM	WS$_2$	ZnSe	FTO
Thickness (nm)	300	100	100	100	50	100	50
Eg (eV)	2.26	3.2	3.05	2.0	1.8	2.81	3.6
χ (eV)	3.69	3.9	4.16	3.9	3.95	4.09	4.0
ε_r	10	9	10	3.9	13.6	8.6	9.0
N$_C$ (cm^{-3})	1×10^{19}	1×10^{21}	5×10^{18}	2.5×10^{21}	2.2×10^{17}	2.2×10^{18}	2.2×10^{18}
N$_V$ (cm^{-3})	1×10^{19}	2×10^{20}	5×10^{18}	2.5×10^{21}	2.2×10^{16}	1.8×10^{18}	1.8×10^{19}
μ_e (cm^2/V s)	7.9×10^{-2}	20	15	0.02	100	400	100
μ_h (cm^2/V s)	7.9×10^{-2}	10	0.1	0.02	100	110	25
N$_D$ (1/cm^3)	1×10^{19}	1×10^{19}	1×10^{17}	2.93×10^{17}	10^{18}	1×10^{15}	5×10^{18}
N$_A$ (cm^{-3})	1×10^{19}	_	_	_	_	_	_
N$_t$ (1/cm^3)	3.5×10^{16}	1×10^{15}	1×10^{15}	1×10^{15}	10^{15}	1×10^{15}	1×10^{14}
Reference	[16]	[19,20]	[21]	[22]	[23]	[18,24]	[25]

Table 3.2: Input parameters for various HTL Materials.

Parameters	Cu$_2$O	CuI	CuSCN	NiO	PEDOT: PSS	Spiro
Thickness (nm)	150	100	100	50	100	200
E$_g$ (eV)	2.17	3.1	3.6	3.6	1.6	3.0
χ (eV)	3.2	2.1	1.7	2.1	3.4	2.2
ε_r	7.1	6.5	10	11.75	3	3.0
N$_C$ (cm^{-3})	2×10^{17}	2.8×10^{19}	2.2×10^{18}	2.5×10^{20}	2.2×10^{18}	2.2×10^{18}
N$_V$ (cm^{-3})	1.1×10^{19}	1×10^{19}	1.8×10^{19}	2.5×10^{20}	1.8×10^{19}	1.8×10^{19}
μ_e (cm^2/V s)	200	100	100	10^{-3}	4.5×10^{-2}	2.10×10^{-3}
μ_h (cm^2/ V s)	80	43.9	25	10^{-3}	4.5×10^{-2}	2.1610^{-3}
N$_D$ (cm^{-3})	_	_	_	_	_	_
N$_A$ (cm^{-3})	1×10^{18}	1×10^{18}	1×10^{18}	1×10^{19}	1×10^{19}	2×10^{19}
N$_t$ (cm^{-3})	1×10^{15}	1×10^{15}	1×10^{15}	1×10^{15}	1×10^{14}	1×10^{15}
Reference	[26]	[27]	[28]	[29]	[30]	[31]

CHAPTER: 4

Results and Discussions

In this study, we analyze the results of all parameters of our proposed PSC model. $(CH_3NH_3)_3Bi_2I_9$ serves as the perovskite layer owing to its non-hazardous nature, excellent stability, and superior optoelectronic characteristics. However, adjusting this perovskite film with suitable ETL and HTL is challenging due to the band structure of the $(CH_3NH_3)_3BI_2I_9$ perovskite layer. However, to achieve the optimum result during simulation, the required configuration FTO/ETL /$(CH_3NH_3)_3BI_2I_9$ /HTL/Pt, for five different ETLs and more than eight HTLs, are taken for simulation, but only six out of them provide more efficient performance. We tested only six HTL materials.

4.1 Optimization of ETLs and HTLs

The optimization of both ETL and HTL of PSCs is vital for achieving a high-performance device, as they significantly influence the device's PCE by regulating electron and hole movement. Fig.4.1 shows the band diagrams of different ETL materials used with $(CH_3NH_3)_3Bi_2I_9$ as the absorber layer, while Fig.4.2 illustrates the band alignment of $(CH_3NH_3)_3Bi_2I_9$ with various HTL materials, providing insight into the energetic compatibility and potential carrier transport across interfaces. By modifying key aspects, including an appropriate band gap, superior carrier mobility, optimal thickness and electron affinity, etc. Fig.4.3 displays the performance parameters of various PSC configurations employing different HTLs like Cu_2O, CuI, CuSCN, PEDOT: PSS, Spiro-OMeTAD, and NiO, where TiO_2 and $(CH_3NH_3)_3BI_2I_9$ serve as ETL and perovskite layer, respectively. Similarly, Fig.4.4 depicts the performance characteristics of various HTLs, where IGZO acts as the ETL alongside a perovskite layer. Figure 4.5 presents the performance parameters of various HTLs using PCBM as ETL, while Figure 4.6 reveals the performance parameters using WS_2 as ETL. Finally, Figure 4.7 also shows the performance parameter of different HTLs with ZnSe as the ETL. In Figure 4.6, after the investigation, it has been determined that the FTO/WS_2/$(CH_3NH_3)_3BI_2I_9$ /NiO/Pt configuration offers the best photo-voltaic parameter performance when NiO and WS_2 are used as HTL and ETL. Across Figure 4.3 to

4.7, it is evident that the highest efficiency of 18.14 %, is achieved when NiO and WS_2 are used as HTL and ETL material respectively, with $(CH_3NH_3)_3BI_2I_9$ serving as the absorber layer in the PSC. However, Cu_2O also demonstrates a notable PCE of over 15% using the same WS_2 as the ETL and $(CH_3NH_3)_3BI_2I_9$ as the absorber layer. The maximum performance is achieved using the configuration $FTO/WS_2/(CH_3NH_3)_3BI_2I_9$ /NiO/Pt. In addition, all simulated results for different cell structures with multiple arrangements of different ETLs and NiO as HTL are represented in Table 4.2.
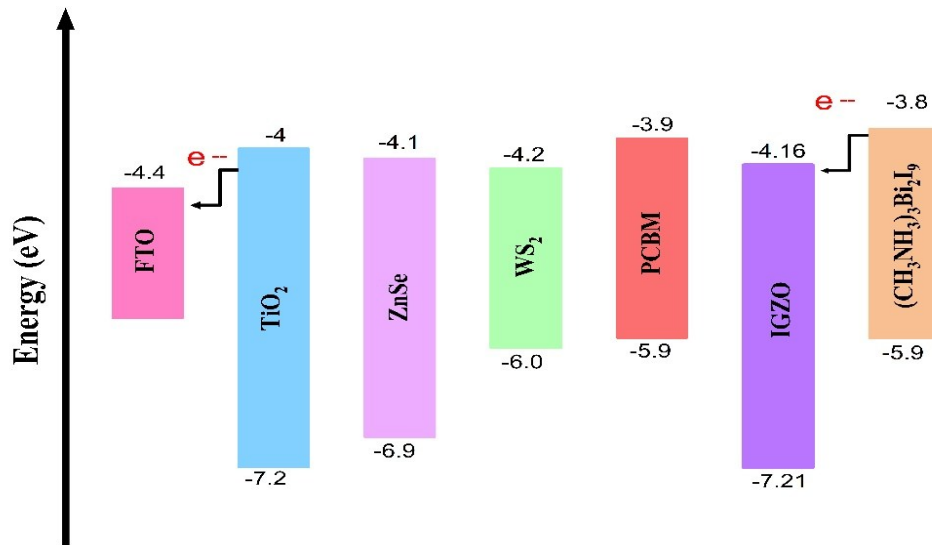

Figure 4.1 Band diagram of different ETL materials with $(CH_3NH_3)_3Bi_2I_9$ as an absorber layer.
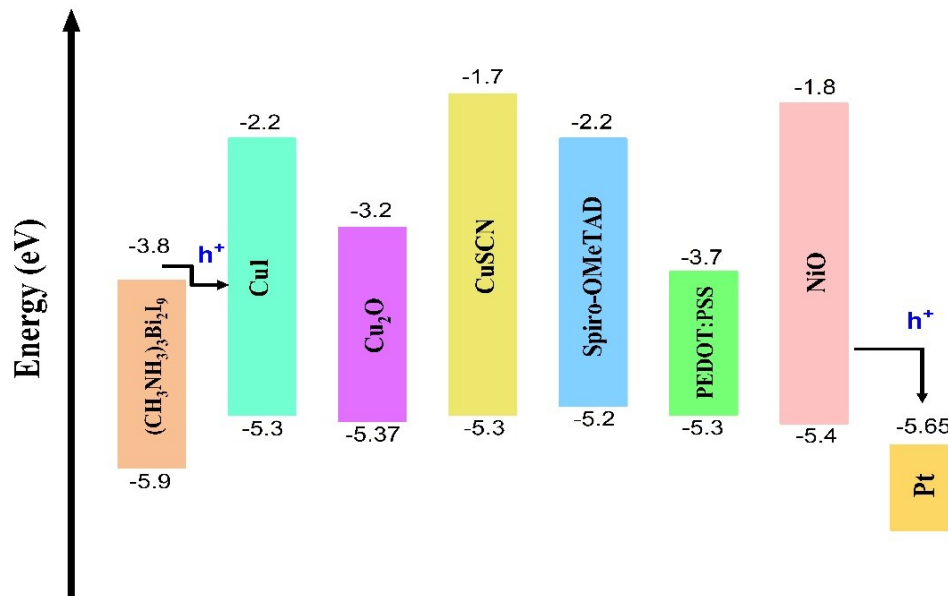

Figure 4.2 Band diagram of $(CH_3NH_3)_3Bi_2I_9$, as an absorber layer with different HTL materials.

Parameters	Cu2O	CuI	CuSCN	POEDOT	Spiro	NiO
Voc (V)	1.687	1.685	1.685	1.703	1.685	1.68
Jsc (mA/cm2)	10.671	10.244	10.241	10.392	10.243	10.25
FF (%)	70.69	59.25	66.11	58	66.04	85.06
pce (%)	12.73	10.23	11.41	10.26	11.41	14.65
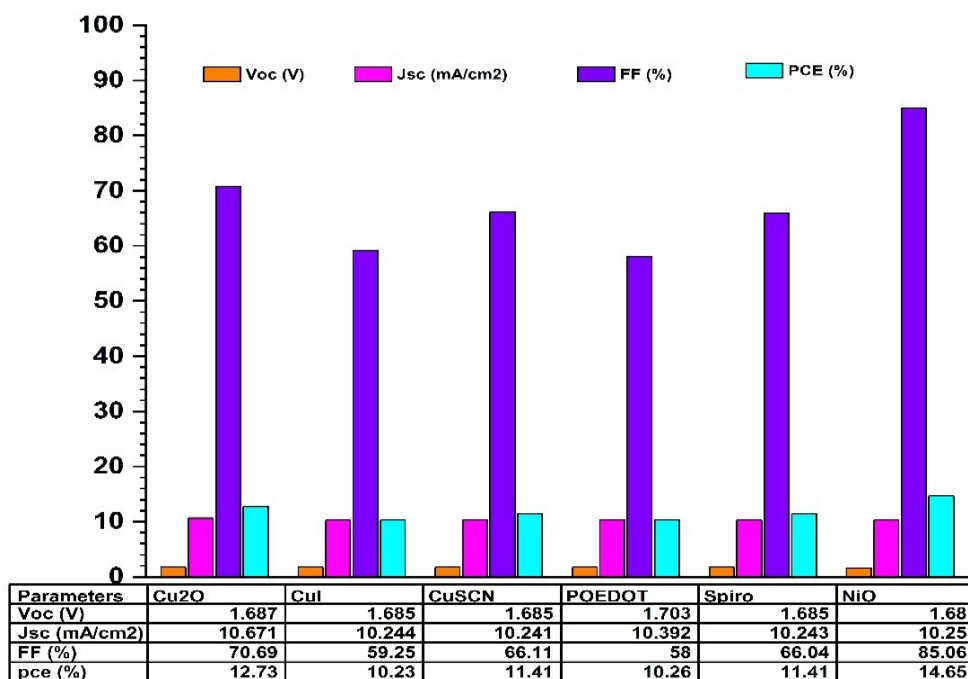
Figure 4.3 Performance parameters of various HTLs with TiO2 as ETL and (CH3NH3)3Bi2I9 as the perovskite layer

Parameters	Cu2O	CuI	CuSCN	PEDOT	Spiro	NiO
Voc (V)	1.682	1.694	1.693	1.711	1.693	1.693
Jsc (mA/cm2)	10.66	10.233	10.234	10.379	10.236	10.251
FF (%)	58.09	46.77	53.34	45.66	53.31	71.41
PCE (%)	10.41	8.11	9.24	8.12	9.24	12.39
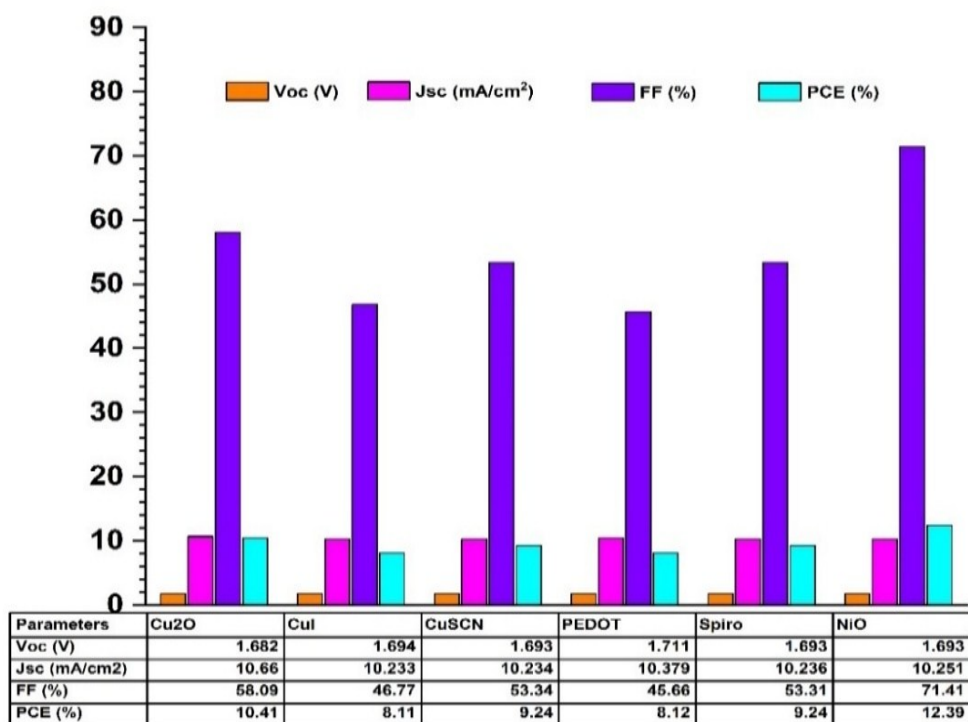
Figure 4.4 Performance parameters of various HTLs with IGZO as ETL and (CH3NH3)3Bi2I9 as the perovskite layer

Parameters	Cu2O	Cul	CuSCN	PEDOT	Spiro	NiO
Voc (V)	1.478	1.461	1.455	1.441	1.455	1.441
Jsc (mA/cm2)	11.175	10.863	10.899	11.033	10.9	10.948
FF (%)	62.13	45.33	58.01	79.61	57.93	81.58
PCE (%)	10.26	7.19	9.21	12.66	9.19	12.87
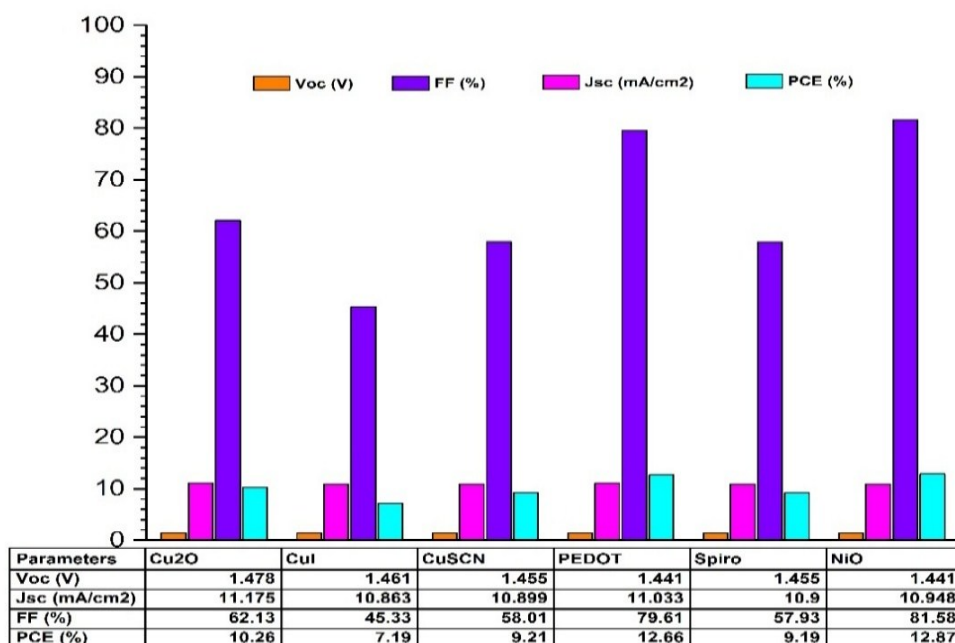
Figure 4.5 Performance parameters of various HTLs with PCBM as ETL and $(CH_3NH_3)_3Bi_2I_9$ as the perovskite layer.

Parameter	Cu2O	Cul	CuSCN	PEDOT	Spiro	NiO
Voc (V)	1.675	1.673	1.673	1.344	1.673	1.673
Jsc (mA/cm	12.947	12.702	12.712	14.689	12.712	12.725
FF (%)	69.67	53.78	65.22	65.23	63	85.16
PCE (%)	15.11	11.43	13.87	12.87	13.4	18.14

Figure 4.6 Performance parameters of various HTLs with WS_2 as ETL and $(CH_3NH_3)_3Bi_2I_9$ as the perovskite layer

Figure 4.7 Performance parameters of various HTLs with ZnSe as ETL and $(CH_3NH_3)_3Bi_2I_9$ as the perovskite layer.

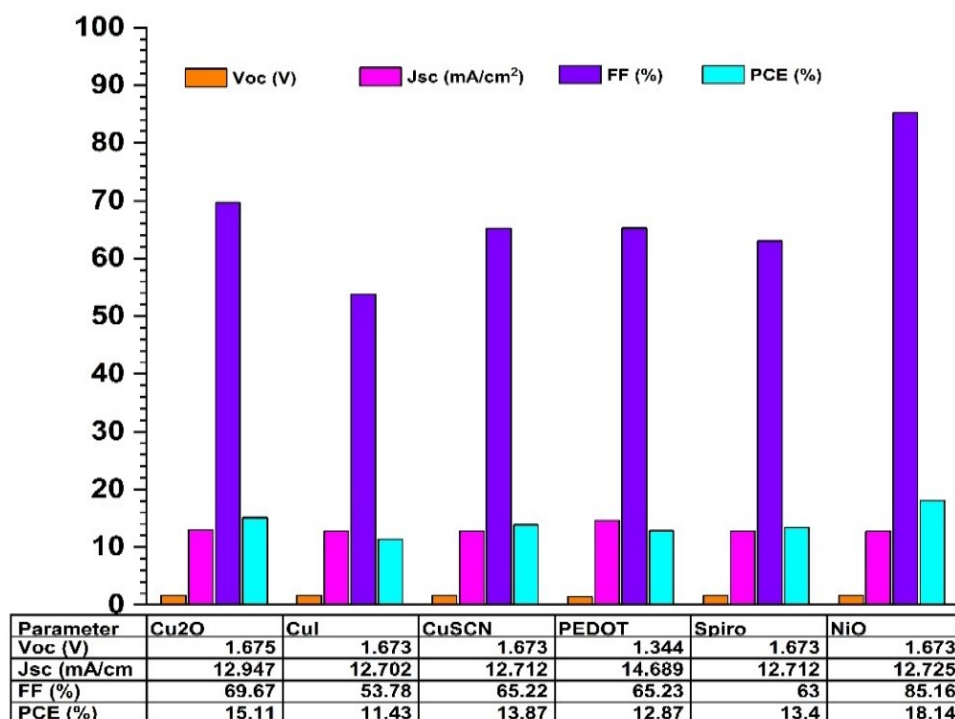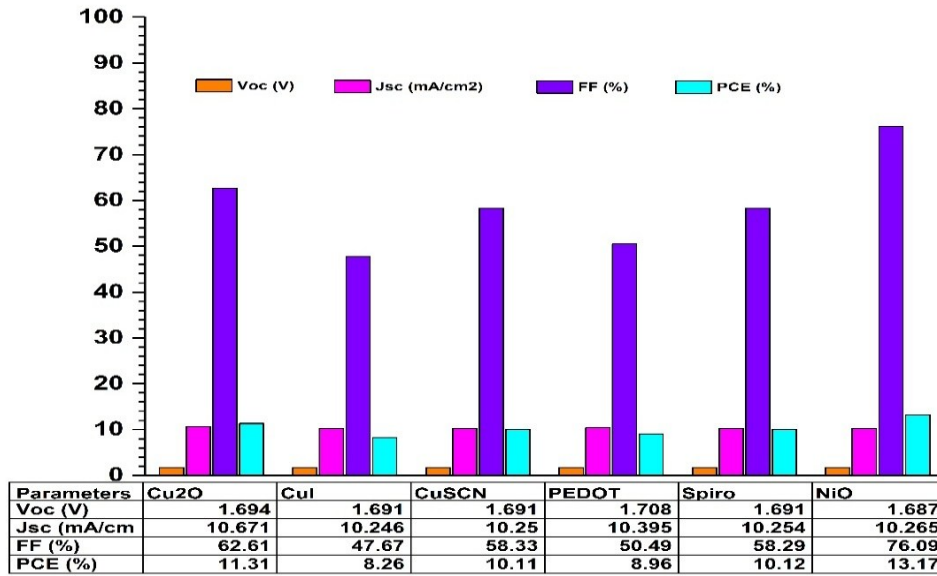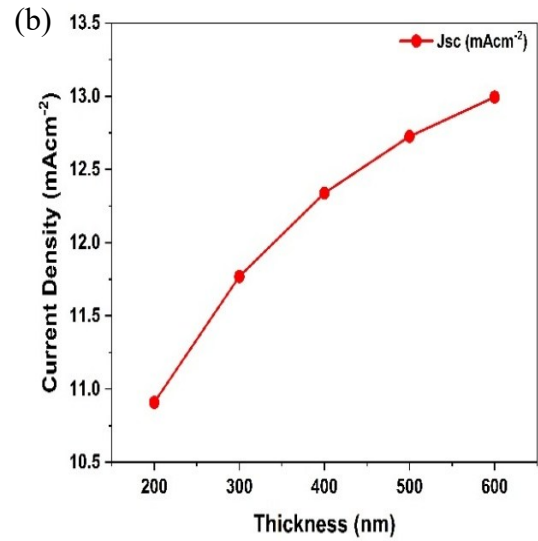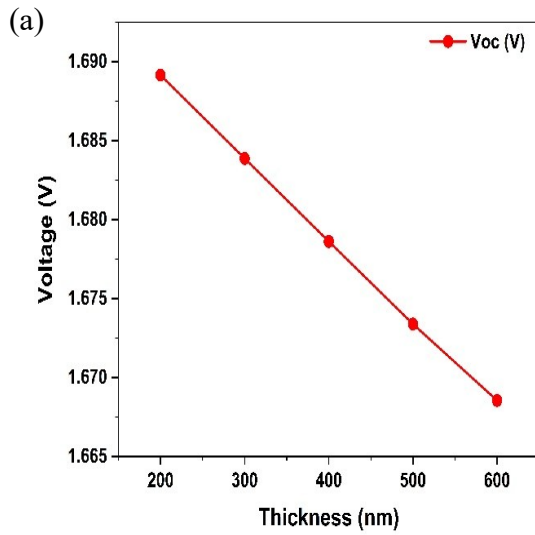## 4.2 Effect of the Perovskite Layer Thickness

The thickness of the perovskite layer significantly impacts the performance of a PSC. The layer thickness can influence its optoelectronic properties through factors like film morphology, directly impacting the photo-generated charge carriers, their lifetime, and diffusion length [31]. To study the significant performance of solar cells, the thickness of the $(CH_3NH_3)_3BI_2I_9$, perovskite film ranges from 200 to 600 (nm). Figure 4.8 (a), (b), (c), and (d) represent the variations in P-V parameters V_{OC}, J_{SC}, FF, and PCE respectively, with varying perovskite layer thickness. It has been observed that V_{OC} decreases from 1.68 to 1.66V as the perovskite layer thickness increases. This is because of the increased recombination of charge carriers for which these carriers have to travel a longer path through the perovskite layer to reach the electrodes. However, J_{SC} increases from 10.908 to 12.993 mAcm^{-2} as the increment in thickness of the perovskite layer. Since a broader layer can capture a greater number of incoming photons, leading to the formation of a larger presence of charge carriers. Conversely, the fill factor (FF) decreases from 89.97 to 83.55%, primarily due to an enhancement in series resistance and carrier mobility issues. The highest PCE of 18.14 % is achieved at a Thickness of 500 nm. Beyond this, the PCE decreases, this is because of the increase in radiative recombination [32] and charge transport issues. Table 3. Input parameter for the optimized $(CH_3NH_3)_3BI_2I_9$-based device.

Table 4.1 Input parameter for the optimized $(CH_3NH_3)_3BI_2I_9$-based device

Parameters/Units	FTO	WS$_2$ (ETL)	MA$_3$Bi$_2$I$_9$	NiO (HTL)
Thickness(nm)	50	**100**	**500**	**100**
E$_g$ (eV)	3.6	1.8	**2.1**	3.6
Electron Affinity (χ)	4.5	3.95	3.69	2.6
Dielectric Constant (ε_r)	10	13.6	10	11.75
N$_C$ (cm^{-3})	2×10^{18}	2×10^{18}	1×10^{19}	2.5×10^{20}
N$_V$ (1/cm^3)	1.8×10^{19}	2×10^{18}	1×10^{19}	2.5×10^{20}
Electron Mobility (μ_e)	100	100	7.91×10^{-2}	1×10^{-3}
Hole Mobility (μ_h)	20	100	7.91×10^{-2}	1×10^{-3}
Electron Thermal velocity (cm.s^{-1})	1×10^7	1×10^7	1×10^7	1×10^7
Hole Thermal velocity (cm.s^{-1})	1×10^7	1×10^7	1×10^7	1×10^7
N$_D$ (1/cm^3)	1×10^{18}	1×10^{18}	1×10^{19}	0
N$_A$ (1/cm^3)	0	0	1×10^{19}	1×10^{20}
N$_t$ (1/cm^3)	1×10^{14}	**1×10^{13}**	**1×10^{14}**	**1×10^{14}**

Note: The bolded parameters indicate the optimized input values.

(c)

(d)
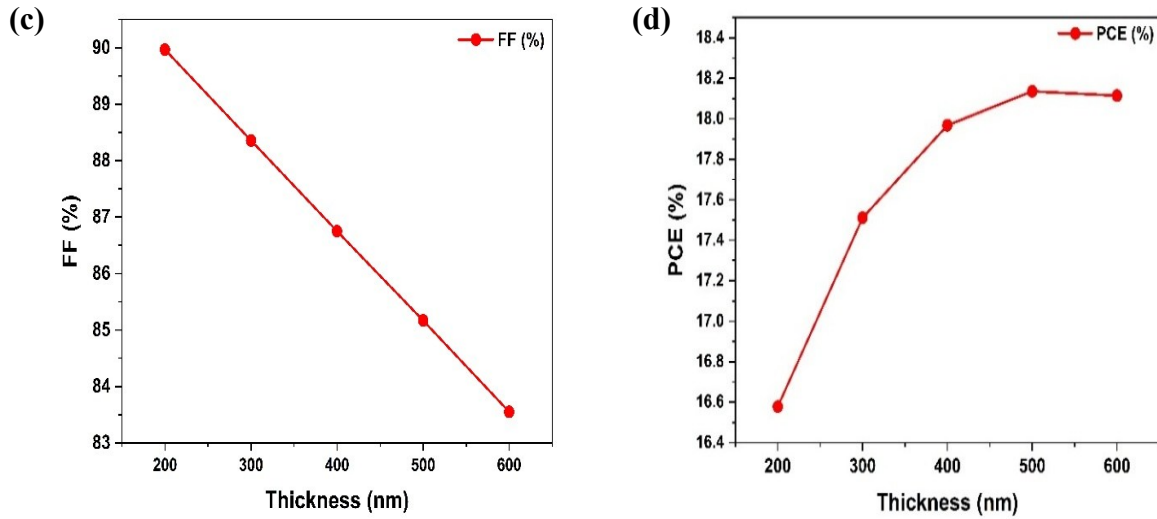
Figure 4.8 Variation of **(a)** V$_{OC}$, **(b)** J$_{SC}$, **(c)** FF, and **(d)** PCE with the changes in the absorber layer thickness.

4.3 Effect of the Bandgap of the perovskite layer

The bandgap energy of the perovskite material significantly influences the performance of the device. A standout feature of PSC is the tunability of the perovskite layer, which has been tuned from 1.9 to 2.2 (eV). Figure 4.9 illustrates the solar cell performance, showing that the maximum V$_{OC}$ of 1.698 V, at a bandgap of 2.2 (eV). Additionally, the highest J$_{SC}$ of 15.559 mAcm^{-2} is noted at a bandgap of 1.9 eV. The optimized values of PCE and FF are 18.14 % and 85.16 %, respectively, at a band gap of 2.1 (eV). However, achieving a lower band gap for this absorber layer is challenging due to the complicated morphology of the (CH$_3$NH$_3$)$_3$Bi$_2$I$_9$ material. Therefore, an energy band gap of 2.1 eV is regarded as the optimized value. Further increasing the bandgap of the perovskite layer causes a drop in PCE and fill factor (FF) due to a reduction in electron generation from photons with higher energy [33]. Whereas a smaller bandgap may result in significant heating losses. The optimized energy bandgap of 2.1 (eV) [34], enables the achievement of a maximum PCE of 18.14 %.
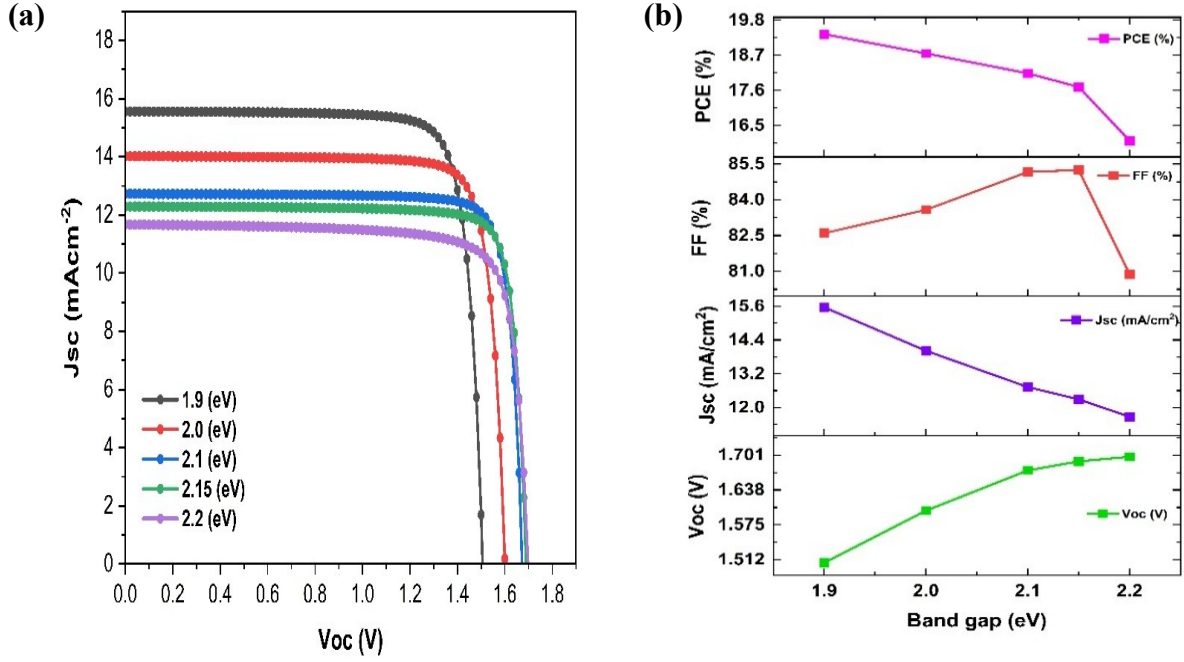
Figure 4.9 J-V Plot and V_{OC}, J_{SC}, FF, and PCE at different band gaps of the Perovskite layer.

4.4 Effect of defect density

The absorber layer significantly influences the efficiency of PSCs. An increase in the defect-density of the $(CH_3NH_3)_3Bi_2I_9$ layer negatively impacts solar cell performance by raising the recombination rates. The Solar cell's performance, after changes in defect-density (N_t), is illustrated in Figure 4.10 (a) and (b). These figures show the changes in the performance parameters including V_{OC}, J_{SC}, PCE, and FF with a simultaneous increase in (N_t) of the perovskite layer. The maximum performance of a PSC is reached at a defect concentration of 10^{14} cm^{-3}. Further ahead, the performance reduces rapidly as (N_t) increases. This decline occurs because a higher (N_t) decreases the distance photo-generated carriers can travel and increases the likelihood of recombination within the perovskite layer [35]. Therefore, maintaining a minimal (N_t) is crucial for facilitating efficient carrier transfer and achieving outstanding photo-voltaic performance in PSCs. Defect density N_t is a key factor in identifying solar cell efficiency, as it significantly influences carrier recombination rates and improves the overall efficiency of PSCs. This study employed simulation-based computation to determine the correlation between photovoltaic parameters and interface defect density at the "WS$_2$ (ETL)/Perovskite" interface, as depicted in Figure 4.11 (c) and (d). Experimentally, interfacial defect densities lying within the range of 10^{11} to 10^{14} cm^{-3} have been reported to enhance PSC performance
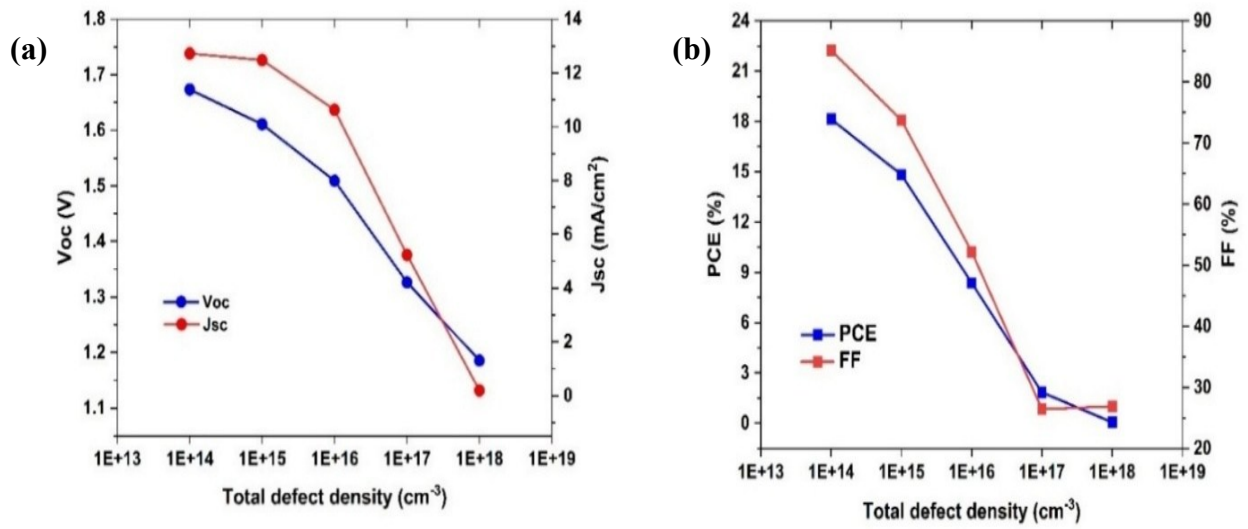
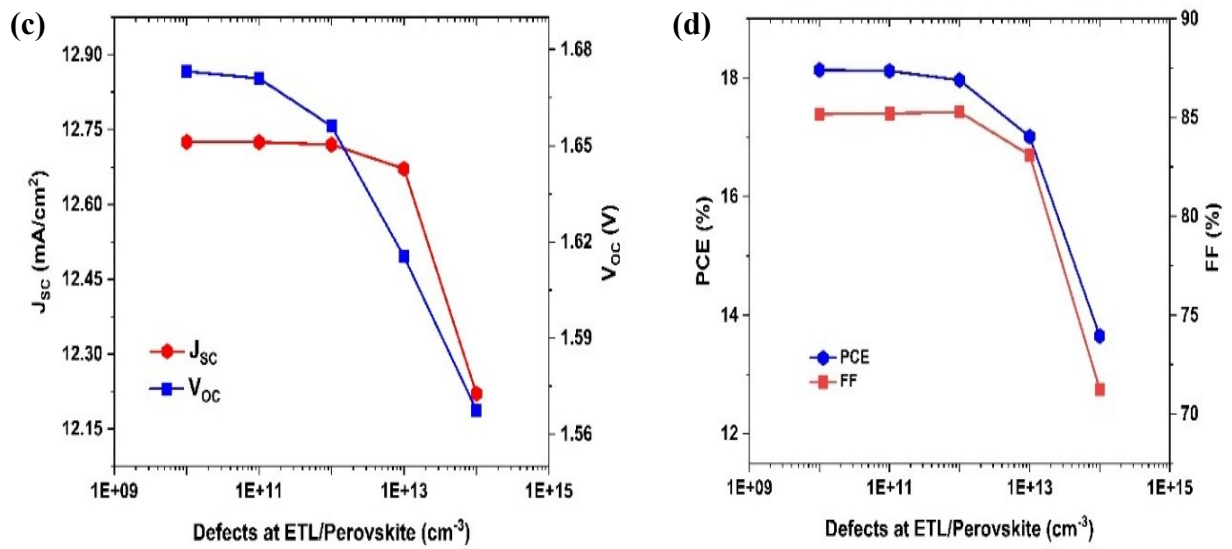**Figure 4.10** The effect of various N_t levels on **(a)** V_{OC}, J_{SC}, and **(b)** PCE, FF.

Figure 4.11 The variation of **(c)** V_{OC}, J_{SC}, and **(d)** PCE, FF for the defects at ETL/Perovskite (cm^{-3}).

4.5 Effect of the Carrier Density

Carrier density in a perovskite solar cell is a crucial factor influencing its performance. The carrier density can be increased through the doping in both ETL and HTL, which are accountable for transporting electrons and holes to the electrodes, respectively. The higher carrier density can enhance the formation of electrons and holes triggered by incident light, bringing about an increase in photovoltaic parameters and overall device efficiency. However, it is essential to maintain a balanced carrier density for optimal PSC performance. Excessively high carrier density may result in greater recombination rates, leading to a decline in device efficiency.

4.5.1 Effect of the Donor density of ETL

To determine the most appropriate doping level of the ETL, the Donor density of WS_2, selected as the ETL in our study, varies from 10^{15} to 10^{19} cm^{-3}. The alteration in key parameters Voc, Jsc, PCE, and FF concerning the donor density of the ETL is represented in Figure 4.12 (a) and (b). With a rise in the donor density of the ETL from 17.39 to 18.12% and FF increased from 82.88 to 84.43 %. The other remaining two parameters in which J_{SC} is almost constant 12.725 to 12.722 mA/cm^2 with donor density, but sudden drop in J_{SC} at donor density 10^{19} cm^{-3}. Moreover, the Voc is enhanced from 1.64 to 1.68 V with increasing the donor density (N_D). The optimized value of N_D is 10^{18} cm^{-3} at which the maximum PCE of 18.14 % has been obtained. Thereafter, a minor drop in PCE at 10^{19} cm^{-3}. By increasing the N_D value, charge generation and transport can be more easily achieved [36].
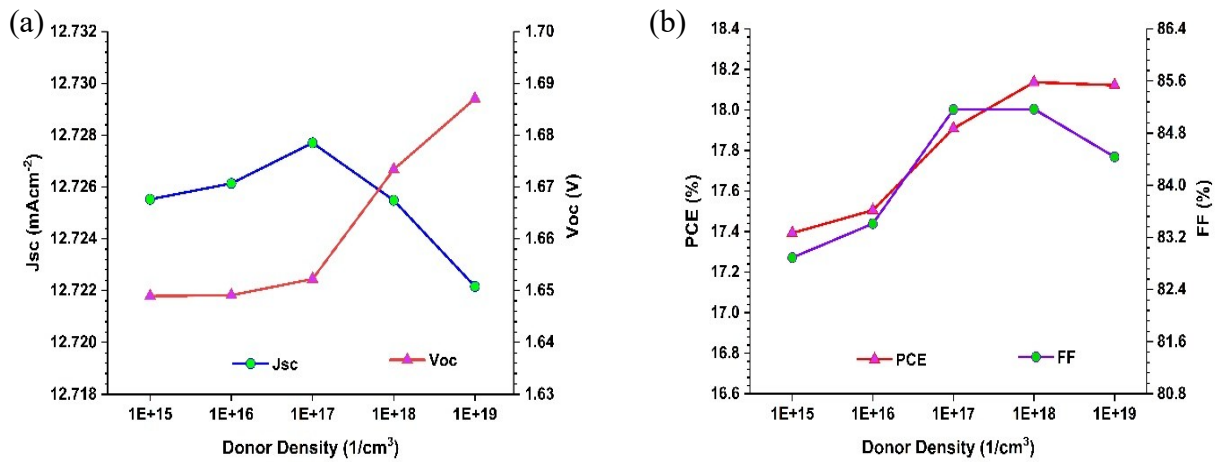

Figure 4.12 The influence of the Donor density of the ETL (WS2) on **(a)** Jsc and Voc, **(b)** FF & PCE.

4.5.2 Effect of the Acceptor density of HTL

The Acceptor density (N_A) of NiO, used as HTL, plays a crucial role in influencing the device's performance. The stability of PSC is influenced by variations in the doping concentration of N_A. To optimize its value, N_A is adjusted from 10^{16} to 10^{21} cm^{-3}. Figures 4.13 (a) and (b) illustrate the variations in photo-voltaic parameters, such as Voc, Jsc, FF, and PCE, as a function of N_A impurity level. Figure 4.13 (a) indicates a little increment in Voc from 1.66 V to 1.67 V and Jsc from 12.718 to 12.725 (mA cm^{-2}), which is observed with an increase in N_A of the HTL. Similarly, as depicted in Figure 4.13 (b), PCE and FF are improved from 17.01 to 18.13 % and 80.13 to 85.16 %, respectively, with variation in N_A from 10^{16} to 10^{21} cm^{-3}. The maximum value of PCE is 18.14 % at N_A of 10^{20} cm^{-3}, therefore, the optimized value of N_A is 10^{20} (1/cm^3). The higher value of N_A can augment the transport of positive charges (holes) within the HTL of PSC which leads to better efficiency of the device [37]. This is due to a decrease in recombination losses and improved charge extraction.
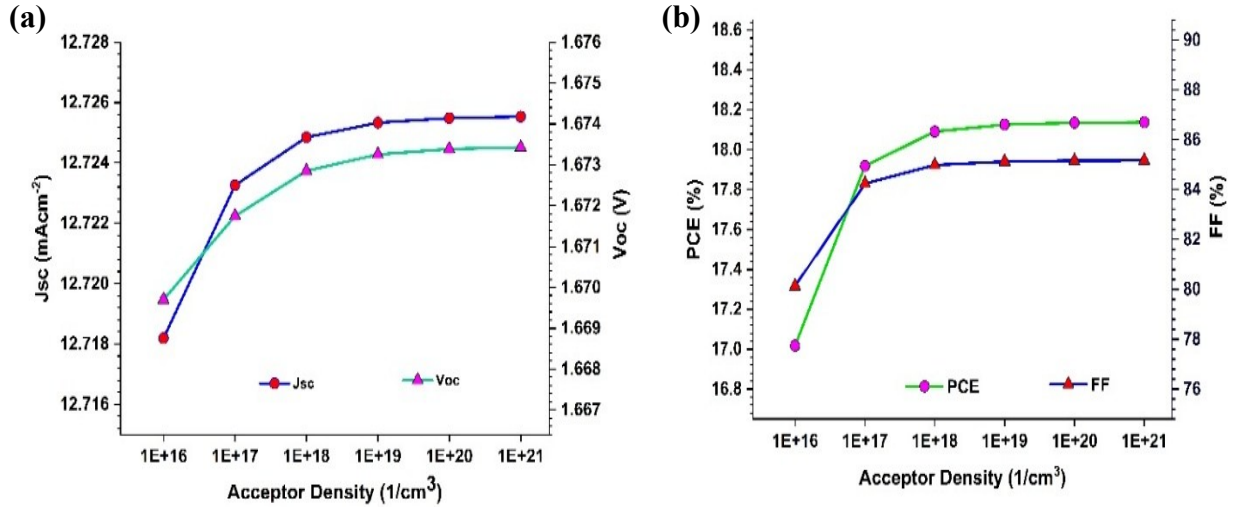

Figure 4.13 The influence of the Acceptor density of the HTL(NiO) on **(a)** Jsc and Voc, **(b)** FF & PCE.

4.6 Effect of the Temperature on the device's performance

The temperature has a significant role in determining the performance of a solar cell. On increasing the temperature, the efficiency of PSC can be reduced because of heightened thermal instability and Deterioration of perovskite material. This study presents the variations in photo-voltaic parameters, including V_{OC}, J_{SC}, FF, and PCE with temperature changes ranging from 300K to 350 K as indicated in Figure 4.14 (a) and (b). The key parameters Voc, Jsc, FF, & PCE decline with temperature rise, indicated by Figure 4.14(b), and on the other side, the variation of temperature on the J-V plot in Figure 4.14(a). This reveals that the lower value of V_{OC} can be observed at a higher temperature. It has been reported that high temperatures can cause phase transition in perovskite material, due to which the structural stability of the material can be affected. An increase in temperature can promote the formation of grain interfaces and introduce defect disorder in the material, contributing to a rise in carrier recombination [38]. These imperfections can lead to a negative impact on the performance of devices.
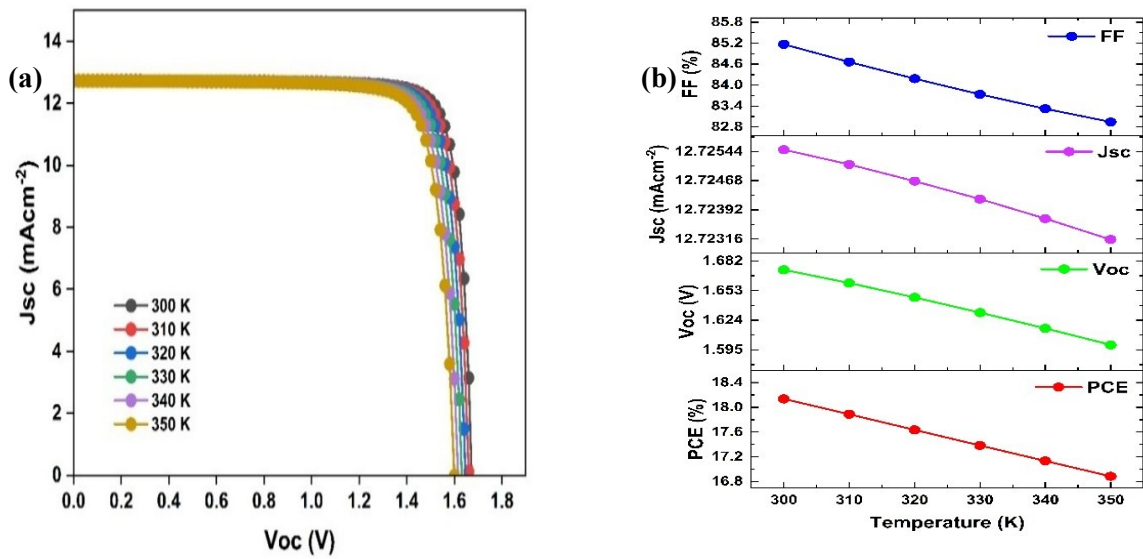

Figure 4.14 (a) Effect of Temperature on J-V curves and **(b)** Characteristics of key parameters, V_{OC}, J_{SC}, FF & PCE.

Table 4.2 Simulated results for different device structures employing various ETLs with NiO as HTL.

Device Structures	Voc (V)	Jsc (mAcm^{-2})	FF (%)	PCE (%)
FTO /TiO$_2$ / (CH$_3$NH$_3$)$_3$Bi$_2$I$_9$/NiO/Pt	1.680	10.25	85.06	14.65
FTO/ZnSe/ (CH$_3$NH$_3$)$_3$Bi$_2$I$_9$/NiO/Pt	1.687	10.265	76.09	13.17
FTO/PCBM/ (CH$_3$NH$_3$)$_3$Bi$_2$I$_9$/NiO/Pt	1.441	10.948	81.58	12.87
FTO/WS$_2$/ (CH$_3$NH$_3$)$_3$Bi$_2$I$_9$/NiO/Pt	1.673	12.725	85.16	**18.14**
FTO/ IGZO/ (CH$_3$NH$_3$)$_3$Bi$_2$I$_9$/NiO/Pt	1.693	10.251	71.41	12.39

4.7 Comparison of the initial and optimized devices

A comparison of the perovskite solar cell (PSC) performance before and after optimization is presented in Figure 4.15, highlighting a significant improvement in the J-V characteristics and QE after optimization. Figure 4.15(a) shows the key performance parameters of the PSC. The J-V characteristics clearly demonstrate that the improved model achieves superior current-voltage behaviour compared to the unoptimized model. This is further supported by Table 4.3, which presents the performance parameters of both initial and optimized device structures. Similarly, Figure 4.15(b) shows that the quantum efficiency (QE) of the optimized model exceeds that of the initial PSC model. The QE for both the optimized and initial models is analyzed over a wavelength range of 300nm to 900nm. Within this range, the QE varies due to modifications in key input parameters of the PSC, such as the absorber layer thickness, energy bandgap, defect density (N_t), and carrier concentration. QE reflects the ability of the perovskite solar cell to generate charge carriers in response to incident photons. As depicted in Figure 4.15(b), maximum QE can be achieved by precisely tuning the device parameters. This optimization enhances the production of electron & hole pairs in the perovskite layer, leading to a higher charge carrier production rate and, consequently, improved overall solar cell efficiency. Figure 4.16 illustrates the energy band diagram of the optimized (CH$_3$NH$_3$)$_3$Bi$_2$I$_9$-based PSC, providing further insight into the charge transport mechanism and energy level alignment within the device. Figure 4.17(a) presents the optimized device structure, while Figure 4.17(b) illustrates the corresponding bandgap alignment for the (CH$_3$NH$_3$)$_3$Bi$_2$I$_9$-based PSC, essential for understanding energy level matching across the device architecture.
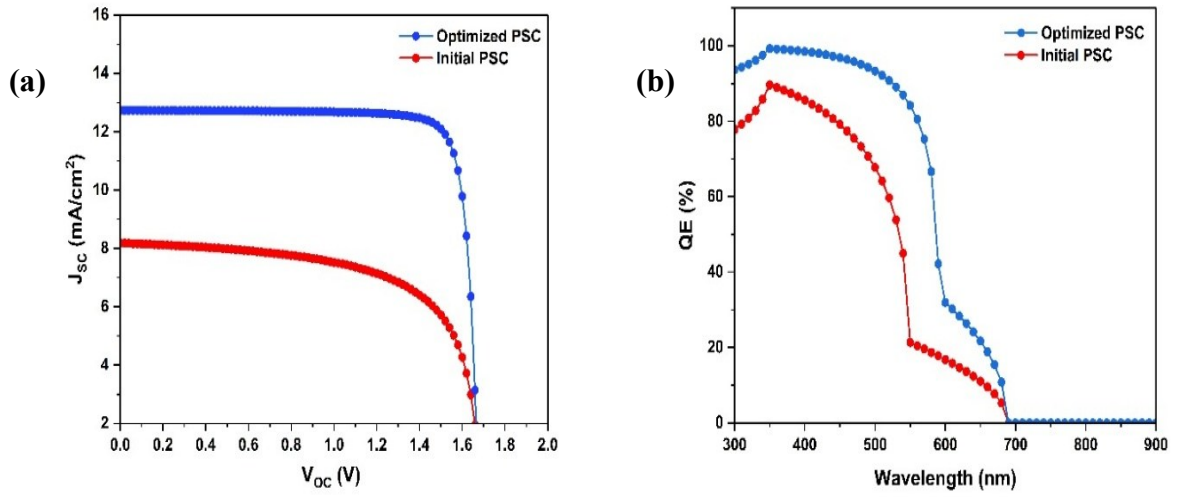
Figure 4.15 (a) J-V Characteristics and **(b)** Q.E. of PSC unoptimized & optimized final model.

Table 4.3 Comparison of P-V parameters of initial and optimised device structure

Parameters	Initial PSC	Optimised PSC
Voc (V)	1.6855	1.6734
Jsc (mA/cm^2)	8.187519	12.731527
FF (%)	65.10	85.17
PCE (%)	8.98	18.14
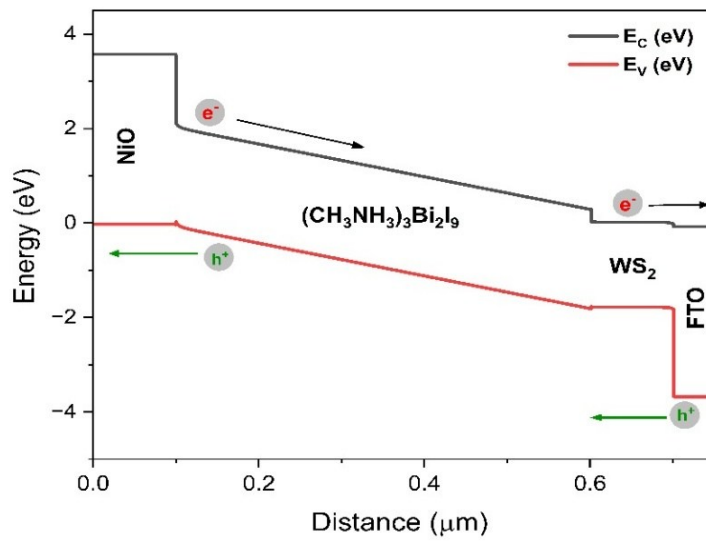
Figure 4.16 Energy band diagram of Optimized (CH$_3$NH$_3$)$_3$Bi$_2$I$_9$-based PSC.
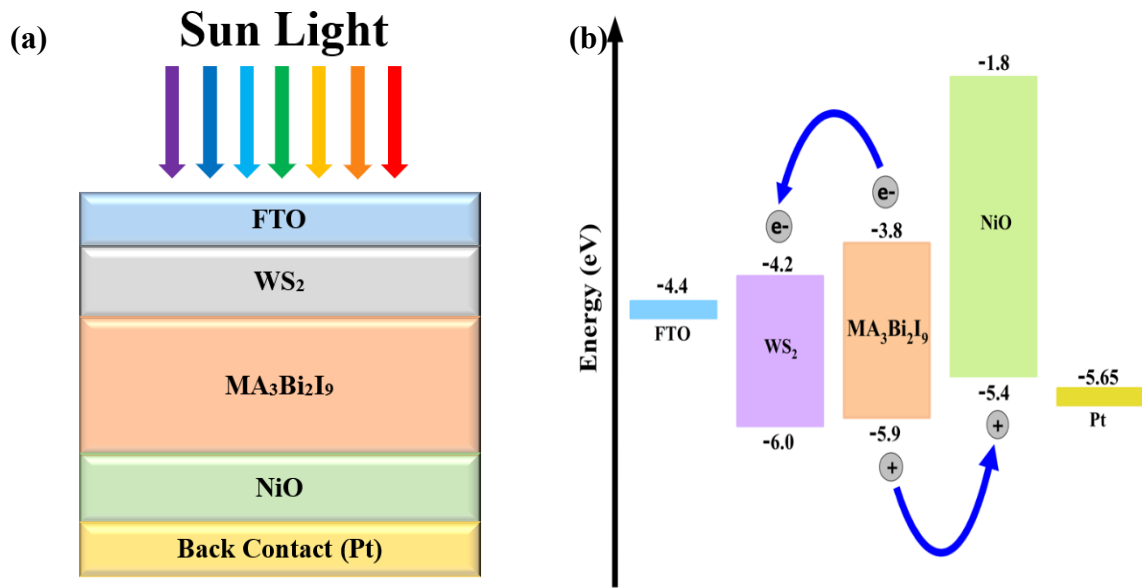
Figure 4.17 (a) Optimized Device Structure and **(b)** Bandgap Alignment for (CH₃NH₃)₃Bi₂I₉-based PSC.

4.8 Comparative study of MBI-based PSC with observed experimental results

Nickel oxide (NiO) is a promising material selected as HTL in PSCs. It can be produced flexibly and this material has an easy manufacturing method, therefor this material is most commonly used in commercial and industrial fields. The NiO material as HTL is suitable for a PSC due to better environmental stability, moderate manufacturing cost, and typically exhibits low mobility in pure form, but doped NiO can significantly improve its hole mobility for use as HTL in PSCs. The tungsten disulfide (WS_2) is used as ETL, and it has high e^--mobility, which helps in improved charge (electron) movement while minimizing recombination losses. WS_2 has a promising energy band gap of 1.8 eV [39], suitable for absorbing a wide range of solar radiation, and is non-toxic, which means beneficial for environmental safety purposes. The designed (CH₃NH₃)₃Bi₂I₉-based PSC model and its simulation show better performance after optimization, which is compared with previously reported results as depicted in Table 4.4.

Table 4.4 Comparison of the simulated MBI-based PSCs with previously reported results.

Authors	Structures	V_{OC} (V)	J_{SC} (mA/cm^2)	FF (%)	PCE (%)
Zhang et al [40]	FTO/c-TiO$_2$/mp-TiO$_2$/ MBI/ Spiro-OMeTAD/Au	0.830	3.000	79.000	1.640
MKA Mohammed [41] (Simulation)	FTO/TiO$_2$/MBI/Spiro-OMeTAD /Au	1.05	10.24	83.65	9.04
Sanjeewani T. Jayawardane [42] (Simulation)	FTO/TiO$_2$/MBI/Spiro-OMeTAD/Au	1.14	18.06	57.33	11.82
Present works (SCAPS-1D Simulation)	FTO/WS$_2$/(CH$_3$NH$_3$)$_3$Bi$_2$I$_9$/NiO/Pt	**1.65**	**12.87**	**85.73**	**18.14**

*ITO: Indium Tin Oxide, PEDOT: PSS Poly(3,4-ethylenedioxythiophene): Poly (styrene sulphonate), PCBM: Phenyl-C61-butyric acid methyl ester.

CHAPTER: 5

My Journey of Learning Through Research Writing

Looking back on my research journey, I am amazed at how much I have learned and grown not just as a student but as a person. When I first started working on my dissertation, I was honestly a bit lost. The world of research, with its unfamiliar methods and technical language, felt overwhelming. I spent hours reading articles, trying to make sense of new concepts, and slowly building up my understanding from the ground up. Before I even began writing my paper, I made it a point to grasp the basics, knowing that a strong foundation was essential.

Throughout this process, I was incredibly lucky to have the support of my dissertation supervisor, Dr. Sarita Baghel. Their patience and guidance helped me navigate both the theoretical and practical sides of my project, especially as I explored the fascinating area of perovskite solar cells. Whenever I hit a roadblock or felt stuck, my Ph.D. scholar, Dr. Rahul Kundara, was always there to offer advice, encouragement, and hands-on help. Their mentorship made a huge difference, giving me the confidence to keep going even when things got tough.

Both my supervisor and Ph.D. scholar also taught me the importance of approaching research and writing in a structured way. They showed me how to break down complex tasks, review my drafts carefully, and stay organized throughout the process. Thanks to their guidance, I was able to complete and submit my research paper for publication—a goal that once seemed out of reach.

This journey has been more than just an academic exercise; it has been a real lesson in perseverance, patience, and the value of having mentors who genuinely care. I'm deeply grateful to my supervisor and Dr. Kundara for their invaluable support and motivation. Their belief in me helped turn a daunting challenge into a rewarding and transformative experience.

CHAPTER: 6

Conclusion

This study presents the modeling and performance analysis of MBI perovskite solar cell using the SCAPS-1D software. The results demonstrate that MBI, possessing a bandgap of 2.1 eV, is an appropriate Pb-free absorber layer. The selection of this layer is due to its exceptional stability and non-toxicity for PSC applications. TiO_2, ZnSe, PCBM, IGZO, and WS_2 are used as ETL material, and Cu_2O, CuI, Spiro-OMeTAD, CuSCN, PEDOT: PSS, and NiO are used as HTL material. Additionally, platinum (Pt) is taken as the metal back contact. A distinctive configuration for the PSC model involved the use of WS_2 as the ETL and NiO as the HTL, combined with the $(CH_3NH_3)_3Bi_2I_9$ perovskite layer. To enhance the performance, the layer thickness is changed from 200nm to 600nm, and the best efficiency of 18.14 % (with Voc of 1.67 V, Jsc of 12.72 mAcm^{-2} and FF is 85.16 %) obtained at a thickness of 500 nm, N_t of 10^{14} 1/cm^3 and temperature of 300K for the configuration of $FTO/WS_2/(CH_3NH_3)_3Bi_2I_9/NiO/Pt$. The maximum PCE is obtained with the N_D of ETL at 10^{18} (1/cm^3). The optimized acceptor density of HTL is 10^{20} cm^{-3}. The performance of the MBI-based PSC has been significantly enhanced, which is applicable for the production of cost-effective PSC devices.

CHAPTER: 7

Future Scope

The double perovskite material $(CH_3NH_3)_3Bi_2I_9$ stands out as a promising contender for advancing solar cell technology. A simulated power conversion efficiency of 18.14%, achieved using SCAPS-1D software, highlights its significant potential. Moving forward, research can aim to enhance the material's structural quality, chemical stability, and film uniformity to support long-term device performance. Addressing the challenges of large-scale production will also be crucial to make this technology commercially viable. Furthermore, integrating $(CH_3NH_3)_3Bi_2I_9$ into tandem architectures could unlock even greater efficiencies by pairing it with complementary absorbers. Inspired by these possibilities, I am eager to investigate this material experimentally to validate its simulated potential and contribute to developing efficient, lead-free, and cost-effective solar solutions.

REFERENCES

1. F. Zafar, M. Khalid, N. Ahmed, M. Tanveer, H. Khalid, R.S. Khan, K. Ayub, Designing spiro-bifluorene core-based promising molecules with enhanced optoelectronic attributes for high-efficiency solar cell devices. Mol. Phys. 121, (2023). https://doi.org/10.1080/00268976.2023.2231571.

2. L. Dou, Y. Yang, J. You, Z. Hong, W.-H. Chang, G. Li, Y. Yang, Solution-processed hybrid perovskite photodetectors with high detectivity. Nat. Commun. 5, 5404 (2014). https://doi.org/10.1038/ncomms6404.

3. A. Kojima, K. Teshima, Y. Shirai, T. Miyasaka, Organometal halide perovskites as visible-light sensitizers for photovoltaic cells. J. Am. Chem. Soc. 131, 6050–6051 (2009). https://doi.org/10.1021/ja809598r.

4. Z. Chen, J.J. Wang, Y. Ren, C. Yu, K. Shum, Schottky solar cells based on CsSnI3 thin-films. Appl. Phys. Lett. 101, 093901 (2012). https://doi.org/10.1063/1.4748888.

5. N.K. Noel, S.D. Stranks, A. Abate, C. Wehrenfennig, S. Guarnera, A. Haghighirad, A. Sadhanala, G.E. Eperon, S.K. Pathak, M.B. Johnston, A. Petrozza, L.M. Herz, H.J. Snaith, Lead-free organic–inorganic tin halide perovskites for photovoltaic applications. Energy Environ. Sci. 7, 3061–3068 (2014). https://doi.org/10.1039/C4EE01076K.

6. F. Hao, C.C. Stoumpos, D.H. Cao, R.P.H. Chang, M.G. Kanatzidis, Lead-free solid-state organic–inorganic halide perovskite solar cells. Nat. Photonics 8, 489–494 (2014). https://doi.org/10.1038/nphoton.2014.82.

7. H. Dammak, A. Yangui, S. Triki, Y. Abid, H. Feki, Structural characterization, vibrational, optical properties and DFT investigation of a new luminescent organic–inorganic material: (C6H14N)3Bi2I9. J. Lumin. 161, 214–220 (2015). https://doi.org/10.1016/j.jlumin.2015.01.010.

8. M. Lyu, J. Pan, X. Ma, Y. Wu, A. Wang, Organic–inorganic bismuth (III)-based material: A lead-free, air-stable and solution-processable light-absorber beyond organo-lead perovskites. Nano Res. 9, 692–702 (2016). https://doi.org/10.1007/s12274-015-0948-y.

9. B. Park, B. Philippe, X. Zhang, H. Rensmo, G. Boschloo, E.M.J. Johansson, Bismuth-based hybrid perovskites A3Bi2I9 (A: methylammonium or caesium) for solar cell application. Adv. Mater. 27, 6806–6813 (2015). https://doi.org/10.1002/adma.201501978.

10. S. Banik, A. Das, B.K. Das, N. Islam, Numerical simulation and performance optimization of a lead-free inorganic perovskite solar cell using SCAPS-1D. Heliyon. 10, e23985 (2024). https://doi.org/10.1016/j.heliyon.2024.e23985.

11. I. Benabdallah, M. Boujnah, A. El Kenz, A. Benyoussef, M. Abatal, A. Bassam, Lead-free perovskite-based bismuth for solar cells absorbers. J. Alloys Compd. 773, 796–801 (2019). https://doi.org/10.1016/j.jallcom.2018.09.332.

12. S. Öz, M. Göksel, N. Tetik, S. Balci, Zero-dimensional (CH3NH3)3Bi2I9 perovskite for optoelectronic applications. Sol. Energy Mater. Sol. Cells. 158, 195–201 (2016). https://doi.org/10.1016/j.solmat.2016.01.035.

13. F. Li, H. Fan, P. Wang, X. Li, Y. Song, K.-J. Jiang, Improved film morphology of (CH3NH3)3Bi2I9 via cation displacement approach for lead-free perovskite solar cells. J. Mater. Sci. 54, 10371–10378 (2019). https://doi.org/10.1007/s10853-019-03582-w.

14. E. Danladi, P.M. Gyuk, N.N. Tasie, A.C. Egbugha, D. Behera, I. Hossain, I.M. Bagudo, M.L. Madugu, J.T. Ikyumbur, Impact of hole transport material on perovskite solar cells with different metal electrode: A SCAPS-1D simulation insight. Heliyon. 9, e16838 (2023). https://doi.org/10.1016/j.heliyon.2023.e16838.

15. A. Rajib, M. A. al Kafi, M. M. H. Najesh, M. R. Hasan, M. R. Miah, A. Rahman, Performance analysis of p-MoTe$_2$/n-MoSe$_2$-based bifacial solar cells with p$^+$-N:Cu$_2$O as BSF layer by SCAPS-1D. Phys. Scr. **99**, 055541 (2024). https://doi.org/10.1088/1402-4896/ad3685.

16. M.K.A. Mohammed, Optimizing non-toxic (CH$_3$NH$_3$)3Bi$_2$I$_9$ perovskite solar cells by SCAPS-1D. Phys. Scr. 99, 125980 (2024). https://doi.org/10.1088/1402-4896/ad9221.

17. S. Banik, A. Das, B.K. Das, N. Islam, Numerical simulation and performance optimization of a lead-free inorganic perovskite solar cell using SCAPS-1D. Heliyon. 10, e23985 (2024). https://doi.org/10.1016/j.heliyon.2024.e23985.

18. V. Deswal, S. Kaushik, R. Kundara, S. Baghel, Numerical simulation of highly efficient Cs2AgInBr6-based double perovskite solar cell using SCAPS 1-D. Mater. Sci. Eng. B. 299, 117041 (2024). https://doi.org/10.1016/j.mseb.2023.117041.

19. M.D. Stamate, On the dielectric properties of DC magnetron TiO2 thin films. Appl. Surf. Sci. 218, 318–323 (2003). https://doi.org/10.1016/S0169-4332(03)00624-X.

20. A. Husainat, W. Ali, P. Cofie, J. Attia, J. Fuller, Simulation and analysis of methylammonium lead iodide (CH3NH3PbI3) perovskite solar cell with Au contact using SCAPS 1D simulator. Am. J. Opt. Photonics. 7, 33 (2019). https://doi.org/10.11648/j.ajop.20190702.12.

21. K.D. Jayan, V. Sebastian, Comprehensive device modelling and performance analysis of MASnI3-based perovskite solar cells with diverse ETM, HTM, and back metal contacts. Sol. Energy. 217, 40–48 (2021). https://doi.org/10.1016/j.solener.2021.01.058.

22. N. Lakhdar, A. Hima, Electron transport material effect on performance of perovskite solar cells based on CH3NH3GeI3. Opt. Mater. 99, 109517 (2020). https://doi.org/10.1016/j.optmat.2019.109517.

23. N. Rai, S. Rai, P.K. Singh, P. Lohia, D.K. Dwivedi, Analysis of various ETL materials for an efficient perovskite solar cell by numerical simulation. J. Mater. Sci. Mater. Electron. 31, 16269–16280 (2020). https://doi.org/10.1007/s10854-020-04263-5.

24. N.K. Sinha, D.S. Ghosh, A. Khare, Role of built-in potential over ETL/perovskite interface on the performance of HTL-free perovskite solar cells. Opt. Mater. 129, 112517 (2022). https://doi.org/10.1016/j.optmat.2022.112517.

25. Y. Xiao, H. Wang, H. Kuang, Numerical simulation and performance optimization of Sb2S3 solar cell with a hole transport layer. Opt. Mater. 108, 110414 (2020). https://doi.org/10.1016/j.optmat.2020.110414.

26. S.T. Jan, M. Noman, Exploring the potential of MAGeI3 perovskite cells with novel charge transport material optimization. Optik. 301, 171684 (2024). https://doi.org/10.1016/j.ijleo.2024.171684.

27. M.K. Hossain, M.S. Alam, M.A. Matin, M.S. Mia, M.A. Islam, M.M. Rana, A. Iqbal, An extensive study on multiple ETL and HTL layers to design and simulation of high-performance lead-free CsSnCl3-based perovskite solar cells. Sci. Rep. 13, 2521 (2023). https://doi.org/10.1038/s41598-023-28506-2.

28. Y. Raoui, H. Ez-Zahraouy, N. Tahiri, O. El Bounagui, S. Ahmad, S. Kazim, Performance analysis of MAPbI₃-based perovskite solar cells employing diverse charge selective contacts: Simulation study. Sol. Energy. 193, 948–955 (2019). https://doi.org/10.1016/j.solener.2019.10.009.

29. Y. Wang, Z. Xia, Y. Liu, H. Zhou, Simulation of perovskite solar cells with inorganic hole transporting materials. IEEE 42nd Photovolt. Spec. Conf. (PVSC). 42, 1–4 (2015). https://doi.org/10.1109/PVSC.2015.7355717.

30. P. Subudhi, D. Punetha, Pivotal avenue for hybrid electron transport layer-based perovskite solar cells with improved efficiency. Sci. Rep. 13, 19485 (2023). https://doi.org/10.1038/s41598-023-33419-1.

31. H. Kim, K.-G. Lim, T.-W. Lee, Planar heterojunction organometal halide perovskite solar cells: roles of interfacial layers. Energy Environ. Sci. 9(1), 12–30 (2016). https://doi.org/10.1039/C5EE02194D.

32. I. Alam, M.A. Ashraf, Effect of different device parameters on tin-based perovskite solar cell coupled with In2S3 electron transport layer and CuSCN and Spiro-OMeTAD alternative hole transport layers for high-efficiency performance. Energy Sources Part A. 46(1), 17080–96 (2024). https://doi.org/10.1080/15567036.2020.1820628.

33. Sadanand, D.K. Dwivedi, Modeling of photovoltaic solar cell based on CuSbS2 absorber for the enhancement of performance. IEEE Trans. Electron Devices. 68(3), 1121–28 (2021). https://doi.org/10.1109/TED.2020.3048326.

34. X. Zhang, C. Wu, J. Wu, H. Zhu, H. Liu, J. Zhu, H. Wang, Active-layer evolution and efficiency improvement of (CH3NH3)3Bi2I9-based solar cell on TiO2-deposited ITO substrate. Nano Res. 9(10), 2921–2930 (2016). https://doi.org/10.1007/s12274-016-1177-8.

35. A. Ghosh, T. Sharma, R. Yadav, S. Banik, N. Islam, Enhancing solar cell efficiency beyond 27% through the implementation of an efficient charge transport layer utilizing an innovative inorganic perovskite Sr3PI3. J. Phys. Chem. Solids. 190, 112029 (2024). https://doi.org/10.1016/j.jpcs.2024.112029.

36. A. Mohandes, M. Moradi, H. Nadgaran, Numerical simulation of inorganic Cs2AgBiBr6 as a lead-free perovskite using device simulation SCAPS-1D. Opt. Quantum Electron. 53(6), 319 (2021). https://doi.org/10.1007/s11082-021-02959-z.

37. A. Sahoo, I. Mohanty, S. Mangal, Effect of acceptor density, thickness and temperature on device performance for tin-based perovskite solar cell. Mater. Today Proc. 62, 6210–15 (2022). https://doi.org/10.1016/j.matpr.2022.05.095.

38. S.M. Jain, N. Kumar, H. Gupta, A. Agarwal, An effective approach of vapour-assisted morphological tailoring for reducing metal defect sites in lead-free (CH3NH3)3Bi2I9 bismuth-based perovskite solar cells for improved performance and long-term stability. Nano Energy. 49, 614–24 (2018). https://doi.org/10.1016/j.nanoen.2018.05.003.

39. K. Sobayel, M.S. Almutairi, M.M. Alotaibi, M.A. Alamri, M.M. Rashid, A comprehensive defect study of tungsten disulfide (WS2) as electron transport layer in perovskite solar cells by numerical simulation. Results Phys. 12, 1097–103 (2019). https://doi.org/10.1016/j.rinp.2018.12.049.

40. Z. Zhang, Y. Liu, Z. Huang, X. Tang, L. Deng, J. Fang, X. Lu, High-quality (CH3NH3)3Bi2I9 film-based solar cells: Pushing efficiency up to 1.64%. J. Phys. Chem. Lett. 8(17), 4300–7 (2017). https://doi.org/10.1021/acs.jpclett.7b01952.

41. M.K.A. Mohammed, Optimizing non-toxic (CH$_3$NH$_3$)3Bi$_2$I$_9$ perovskite solar cells by SCAPS-1D. Phys. Scr. 99(12), 125980 (2024). https://doi.org/10.1088/1402-4896/ad9221.

42. S.T. Jayawardane, J.P.W. Jayasekara, A.B. Meddegoda, H.A.D. Madugama, A.H. Jayatissa, Simulation-based performance analysis of lead-free bismuth perovskite solar cells: A comparative study of Cs3Bi2I9 and (CH3NH3)3Bi2I9-based perovskite solar cells. Adv. Theory Simul. 7(7), (2024). https://doi.org/10.1002/adts.202400206.

PLAGIARISM REPORT

CHAPTER 1 thesis.docx

Delhi Technological University

Document Details

Submission ID
trn:oid:::27535:99784075

Submission Date
Jun 7, 2025, 10:17 PM GMT+5:30

Download Date
Jun 7, 2025, 10:26 PM GMT+5:30

File Name
CHAPTER 1 thesis.docx

File Size
2.5 MB

37 Pages
8,242 Words
47,617 Characters

---

turnitin   Page 2 of 42 - Integrity Overview   Submission ID trn:oid:::27535:99784075

6% Overall Similarity

The combined total of all matches, including overlapping sources, for each database.

Filtered from the Report

- Bibliography
- Quoted Text
- Cited Text
- Small Matches (less than 10 words)

Exclusions

- 5 Excluded Matches

Match Groups

- 36 Not Cited or Quoted 6%
  Matches with neither in-text citation nor quotation marks
- 0 Missing Quotations 0%
  Matches that are still very similar to source material
- 0 Missing Citation 0%
  Matches that have quotation marks, but no in-text citation
- 0 Cited and Quoted 0%
  Matches with in-text citation present, but no quotation marks

Top Sources

- 3% Internet sources
- 5% Publications
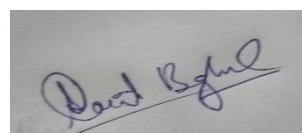- 2% Submitted works (Student Papers)

Integrity Flags

0 Integrity Flags for Review

No suspicious text manipulations found.

Our system's algorithms look deeply at a document for any inconsistencies that would set it apart from a normal submission. If we notice something strange, we flag it for you to review.

A Flag is not necessarily an indicator of a problem. However, we'd recommend you focus your attention there for further review.

Place: Delhi

Date: 09 June 2025

Dr. Sarita Baghel

(Supervisor's Signature)

Match Groups

🔴 **36** Not Cited or Quoted 6%
Matches with neither in-text citation nor quotation marks

🟠 **0** Missing Quotations 0%
Matches that are still very similar to source material

🟡 **0** Missing Citation 0%
Matches that have quotation marks, but no in-text citation

🔵 **0** Cited and Quoted 0%
Matches with in-text citation present, but no quotation marks

Top Sources

3% 🌐 Internet sources

5% 📖 Publications

2% 👤 Submitted works (Student Papers)

Top Sources

The sources with the highest number of matches within the submission. Overlapping sources will not be displayed.

1   Publication

Mustafa K. A. Mohammed. "Optimizing non-toxic (CH3NH3)3Bi2I9 perovskite sola...   <1%

2   Publication

Sujan Banik, Arnob Das, Barun K. Das, Nurul Islam. "Numerical simulation and pe...   <1%

3   Publication

Sumit Singh, Rahul Kundara, Sarita Baghel. " Device modelling and optimization o...   <1%

4   Internet

www.preprints.org   <1%

5   Submitted works

Queensland University of Technology on 2022-06-19   <1%

6   Internet

dspace.univ-msila.dz   <1%

7   Internet

link.springer.com   <1%

8   Submitted works

Islamic University of Technology on 2025-06-02   <1%

9   Submitted works

Berhampur University on 2025-04-03   <1%

10   Publication

Alok Kumar, Sushama M. Giripunje. "A comparative numerical simulation study o...   <1%

11   Publication

Akash Anand Verma, D.K. Dwivedi, Pooja Lohia, Rahul Pandey, Jaya Madan, Surbh...   <1%

12   Publication

M. Shihab Uddin, Md. Abdullah Al Mashud, G. F. Ishraque Toki, Rahul Pandey et al...   <1%

13   Publication

Makambo, John Beya. "Performance and Assessment of Tandem GaInp /GaAs Dua...   <1%

14   Internet

downloads.hindawi.com   <1%

15   Publication

George G. Njema, Vincent Kioko, Bonface N. Mwangi, Joshua K. Kibet. "Design an...   <1%

16   Internet

pmc.ncbi.nlm.nih.gov   <1%

17   Internet

www.rsc.org   <1%

18   Publication

Shazia Akhtar Dar, Brajendra Singh Sengar. "Design and performance optimizatio...   <1%

19   Publication

Shuaibu Sani, Abdullahi Usman, Apichai Bhatranand, Yuttapong Jiraraksopakun, ...   <1%

20   Publication

Ammar Sehili, Abdesselam Bouloufa. "A Theoretical Study to Investigate in Perov...   <1%

21   Publication

Md. Shamim Reza, Avijit Ghosh, Abul Kalam Azad, Md. Selim Reza et al. "Boosting ...   <1%

22   Publication

Shahid Mehmood, Zahid Ali, Shah Rukh Khan, Meznah M. Alanazi, Shaimaa A. M. ...   <1%

23   Internet

eprints.uanl.mx   <1%

24   Internet

ir.jkuat.ac.ke   <1%

APPENDICES

A.1 PROOF OF SUBMISSION AND STATUS OF PAPER:

Transactions on Electrical and Electronic Materials (TEEM) <em@editorialmanager.com>   Mon 5 May, 19:20 ☆ ☺ ↩ ⋮
to me ▾

Re: "Performance optimization of lead-free (CH3NH3)3Bi2I9-based perovskite solar cell: A SCAPS-1D simulation study"
Full author list: Sudhir Kumar; Rahul Kundara; Sarita Baghel

Dear Mr Sudhir Kumar,

We have just received the submission entitled: "Performance optimization of lead-free (CH3NH3)3Bi2I9-based perovskite solar cell: A SCAPS-1D simulation study" for possible publication in Transactions on Electrical and Electronic Materials, and you are listed as one of the co-authors.

The manuscript has been submitted to the journal by Mr Rahul Kundara who will be able to track the status of the paper through his/her login.

If you have any objections, please contact the editorial office as soon as possible. If we do not hear back from you, we will assume you agree with your co-authorship.

Thank you very much.

With kind regards,

Springer Journals Editorial Office
Transactions on Electrical and Electronic Materials

← **Submissions Being Processed for Author**

Page: 1 of 1 (1 total submissions)   Results per page 10 ▾

Action ➕ ▽×	Manuscript Number ▲	Title ▲	Initial Date Submitted ▼	Status Date ▲	Current Status ▲
Action Links	TEEM-D-25-00188	Performance optimization of lead-free (CH3NH3)3Bi2I9-based perovskite solar cell: A SCAPS-1D simulation study	05 May 2025	28 May 2025	Under Review

Status: <u>Under Review</u>

A.2 PROOF OF SCI/SCOPUS/SCIE/ESCI INDEXING:

TRANSACTIONS ON ELECTRICAL AND ELECTRONIC MATERIALS

Publisher: SPRINGER , ONE NEW YORK PLAZA, SUITE 4600 , NEW YORK, United States, NY, 10004

ISSN / eISSN: 1229-7607 / 2092-7592

Web of Science Core Collection: **Emerging Sources Citation Index**

‹ Share This Journal   View profile page